Erratum for the Report “A nontoxic pain killer designed by modeling of pathological receptor conformations” by V. Spahn, G. Del Vecchio, D. Labuz, A. Rodriguez-Gaztelumendi, N. Massaly, J. Temp, V. Durmaz, P. Sabri, M. Reidelbach, H. Machelska, M. Weber, C. Stein

See allHide authors and affiliations

Science 09 Jun 2017:
Vol. 356, Issue 6342, eaao0278
DOI: 10.1126/science.aao0278

- Article
- Info & Metrics
- eLetters

In the Report “A nontoxic pain killer designed by modeling of pathological receptor conformations,” several changes have been made to the text and Fig. 1. On page 966, the author has revised the spelling of the chemical abbreviated as NFEPP, removed “F3* in” before the citation to table S1, and has made two changes to part (C) of Fig. 1 and the corresponding legend. The revised Fig. 1 includes definitions of R1 and R2. In the legend, the chemical name spelling has been corrected again and the sites of fluorination are changed to R1 and R2. In the accompanying Supplementary Materials revision, the authors have explained the experimental procedures regarding the chemical synthesis of NFEPP.

Corrected 8 June 2017. See Erratum.

REPORT

PAIN RESEARCH

A nontoxic pain killer designed by modeling of pathological receptor conformations

V. Spahn,[1]† G. Del Vecchio,[1]† D. Labuz,[1] A. Rodriguez-Gaztelumendi,[1] N. Massaly,[1]* J. Temp,[1] V. Durmaz,[2] P. Sabri,[2] M. Reidelbach,[2] H. Machelska,[1] M. Weber,[2]‡ C. Stein[1]‡§

Indiscriminate activation of opioid receptors provides pain relief but also severe central and intestinal side effects. We hypothesized that exploiting pathological (rather than physiological) conformation dynamics of opioid receptor-ligand interactions might yield ligands without adverse actions. By computer simulations at low pH, a hallmark of injured tissue, we designed an agonist that, because of its low acid dissociation constant, selectively activates peripheral μ-opioid receptors at the source of pain generation. Unlike the conventional opioid fentanyl, this agonist showed pH-sensitive binding, heterotrimeric guanine nucleotide–binding protein (G protein) subunit dissociation by fluorescence resonance energy transfer, and adenosine 3′,5′-monophosphate inhibition in vitro. It produced injury-restricted analgesia in rats with different types of inflammatory pain without exhibiting respiratory depression, sedation, constipation, or addiction potential.

Pain treatment is a major challenge in clinical medicine and public health (*1*). Unfortunately, currently available analgesics are severely limited by adverse effects. Opioids produce sedation, apnea, nausea, addiction, and constipation mediated in brain or gut, and cyclooxygenase inhibitors can elicit ulcers, bleeding, myocardial infarction, or stroke (*2*, *3*). Previous strategies in drug development have focused on central opioid receptors in noninjured environments (*4*, *5*). However, a large number of painful syndromes (e.g., arthritis, neuropathy, and surgery) are driven by peripheral sensory neurons (*6*–*8*) and are typically accompanied by inflammation with tissue acidosis (*9*, *10*). Under such circumstances, peripheral opioid receptors and their signaling pathways are up-regulated and mediate a considerable proportion of opioid analgesia in animals and humans (*11*–*14*). Acidosis can augment the function of heterotrimeric guanine nucleotide–binding protein (G protein)–coupled receptors (GPCRs) (*15*–*19*) and affects the protonation of ligands, which is essential for binding and activation of opioid receptors (*5*, *20*). Current structural information on opioid receptors and ligands is limited to physiological environments (pH 7.4) (*21*–*23*) and therefore calls for the analysis of their pathological conformations. We hypothesized that an agonist designed to selectively activate μ-opioid receptors (MORs) at low pH will not elicit side effects typically mediated by central or intestinal MORs exposed to physiological conditions (*11*, *24*).

In computational simulations, we integrated structural data on MOR (*21*) and its ligand fentanyl (*25*, *26*). Because its logarithmic-scale acid dissociation constant (pK_a) value is above 8 (*27*, *28*), fentanyl is protonated and activates MOR in both normal (pH 7.4) and inflamed (pH 5 to 7) milieus. We hypothesized that a ligand with a pK_a between 6 and 7 should be protonated and able to activate MOR exclusively in inflamed tissue. We simulated the replacement of hydrogens (Fig. 1A) by fluorine (F), which attracts protons and decreases pK_a. In addition, we evaluated binding energies of protonated and deprotonated ligands. The strong interaction between protonated fentanyl and Asp^{147} in MOR was lost without protonation (Fig. 1B). The most promising candidates regarding both quantum-chemically estimated pK_a values (6.73 and 6.93) (table S1) and binding energies (highly negative ΔG values) (table S1) were H-F3 and H-F7 (table S1) (for further details see supplementary materials). Accordingly, the chemical synthesis of (±)-*N*-(3-fluoro-1-phenethylpiperidine-4-yl)-*N*-phenyl propionamide (NFEPP) (Fig. 1C, right; table S1) was carried out by a contractor, and its pK_a was determined experimentally as 6.8.

In binding experiments, inhibition constant (K_i) values of ligands displacing specifically bound [^{3}H][D-Ala^2,*N*-Me-Phe^4,Gly^5-ol]-enkephalin (DAMGO) in MOR-transfected human embryonic kidney (HEK) 293 (HEK293) cells indicated similar affinities of fentanyl across different pH values (Fig. 2A). Conversely, NFEPP affinity dropped at physiological pH compared with acidic conditions

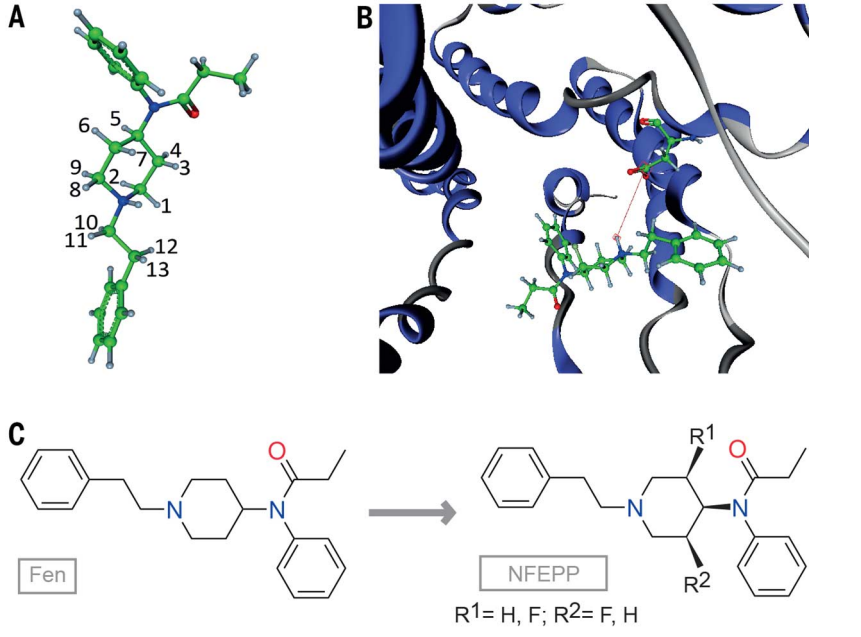

Fig. 1. Computationally based design of fluorinated fentanyl derivatives. (**A**) Fentanyl (Fen) with indexed positions (black numbers) of hydrogen atoms to be substituted with fluorine (F). (**B**) Acidic proton of fentanyl in close vicinity of the nearest side-chain oxygen (red) of Asp^{147} in the μ-opioid receptor (MOR)–binding site. (**C**) Chemical structures of fentanyl (left) and (±)-*N*-(3-fluoro-1-phenethylpiperidine-4-yl)-*N*-phenyl propionamide (NFEPP, right). Sites of fluorination are indicated as R^1 and R^2.

[1]Department of Anesthesiology and Critical Care Medicine, Charité-Universitätsmedizin Berlin Campus Benjamin Franklin, Freie Universität Berlin, Hindenburgdamm 30, Berlin 12203, Germany. [2]Computational Molecular Design, Zuse-Institut Berlin, Takustrasse 7, Berlin, 14195, Germany. *Present address: Washington University Pain Center, Department of Anesthesiology, Washington University School of Medicine, St. Louis, MO 63110, USA. †These authors contributed equally to this work. ‡These authors contributed equally to this work. §Corresponding author. Email: christoph.stein@charite.de

Corrected 8 June 2017. See Erratum.

(Fig. 2B), in line with our simulations (table S1). Shortening incubation times from 90 min (Fig. 2, A and B) to 30 or 15 min (fig. S1) produced similar results.

To assess ligand-induced G-protein activation, we measured the dissociation of G-protein subunits by real-time fluorescence resonance energy transfer (FRET) in HEK293 cells transfected with MOR; the G-protein subunit $G\beta_1$; pertussis toxin (PTX)–resistant $G\alpha_{i1}$mTqΔ6; and Venus-$G\gamma_2$ (fig. S2). All of these were localized at the plasma membrane (fig. S2). The functionality of transfected G-protein subunits was confirmed by persistent fentanyl-induced adenosine 3′,5′-monophosphate (cAMP) inhibition in the presence of PTX. pH-dependent quenching of baseline fluorescence was excluded (fig. S2). Decreasing FRET between $G\alpha_{i1}$mTqΔ6 and Venus-$G\gamma_2$ demonstrated G-protein dissociation upon MOR stimulation. Fentanyl caused energy transfer from the donor-acceptor (DA) to the donor-donor (DD) channel (fig. S2I), resulting in FRET decrease (fig. S2J and Fig. 2, C and E), which indicates G-protein dissociation at both low and normal pH. In contrast, NFEPP caused significant FRET decrease only at low (Fig. 2F), but not at normal, pH (Fig. 2D). G-protein activation by both fentanyl and NFEPP was successfully blocked by the opioid receptor antagonist naloxone (NLX) under all conditions (Fig. 2, C to G). NLX alone did not modulate FRET responses.

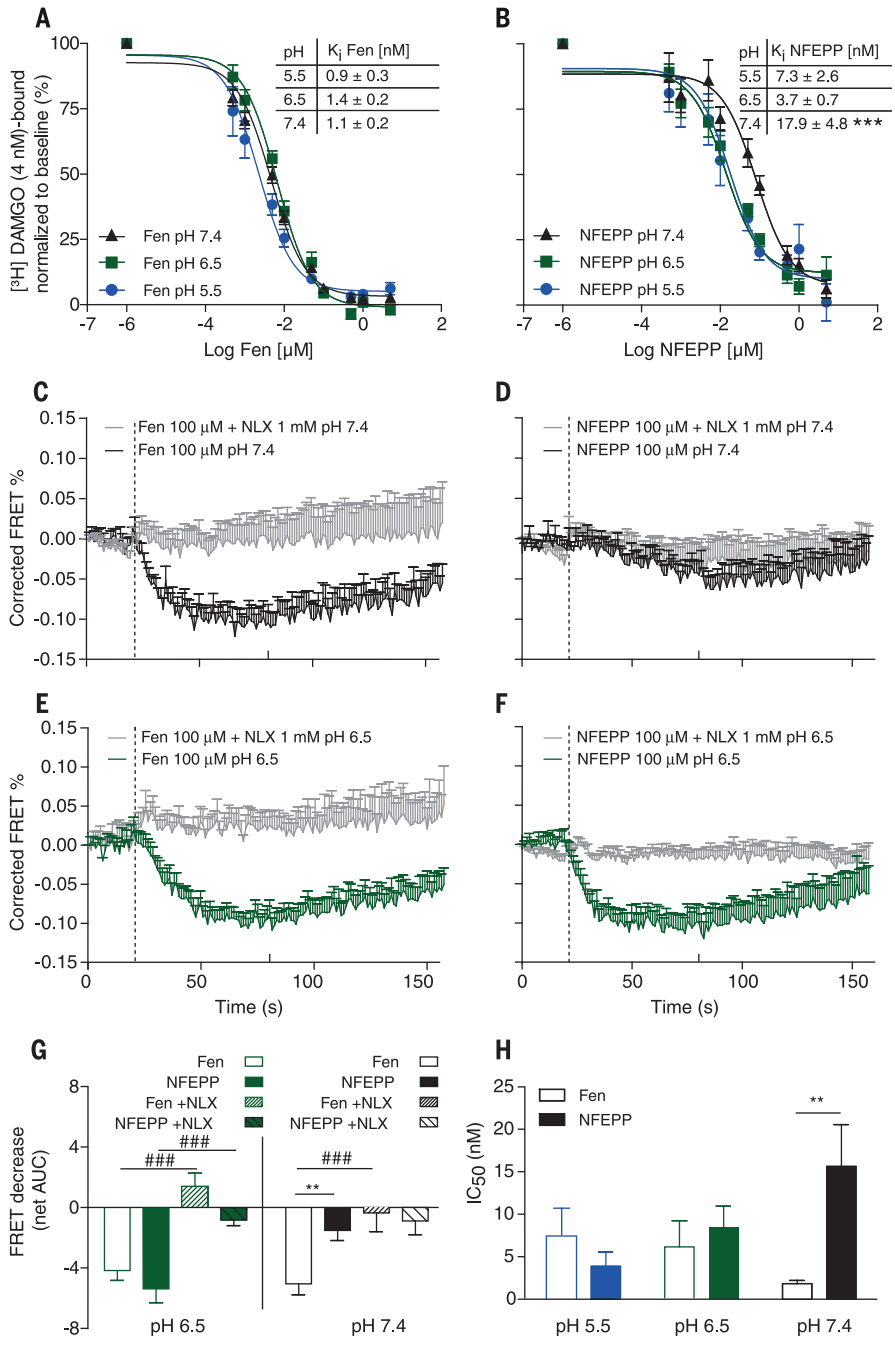

The potency of cAMP inhibition [assessed by half maximal inhibitory concentration (IC_{50}) values calculated from dose-response curves in fig. S3, A and B] induced by fentanyl did not change significantly, whereas those induced by NFEPP decreased with increasing pH values (Fig. 2H). At physiological pH, the potency of NFEPP was more than one order of magnitude less than that of fentanyl. The effects of both fentanyl and NFEPP were reversible by NLX (fig. S3C).

To examine analgesic efficacy in vivo, we tested fentanyl and NFEPP in two clinically relevant rat models of persistent or acute inflammatory pain, i.e., unilateral hindpaw inflammation at 4 days after intraplantar (i.pl.) injection of complete Freund's adjuvant (CFA), or at 2 hours after plantar incision (see supplementary materials). Tissue pH values were significantly decreased in injured compared with noninjured paws, both after CFA (6.8 ± 0.02 versus 7.2 ± 0.03, $P < 0.0001$, paired t test) and incision (7.02 ± 0.02 versus 7.2 ± 0.01, $P < 0.0001$, paired t test). After CFA injection, rats developed overt paw inflammation (redness and swelling), reduced paw pressure thresholds (PPTs) ("hyperalgesia") (Fig. 3A and fig. S4), reduced paw withdrawal thresholds to von Frey filaments (PWTs or "allodynia") (Fig. 3B and fig. S4), and reduced paw withdrawal latencies (PWLs) to heat stimulation ("thermal hypersensitivity") (Fig. 3C and fig. S4) in ipsilateral compared with contralateral paws. Fentanyl [2 to 12 μg per kg body weight, administered intravenously (i.v.)] produced analgesia, as demonstrated by dose-dependent elevation of nociceptive thresholds in inflamed ("injured") and in contralateral ("noninjured") paws (Fig. 3 and fig. S4). In contrast, NFEPP (2 to 12 μg/kg i.v.) produced dose-dependent analgesia only in inflamed paws (Fig. 3 and fig. S4). At 8 to 12 μg/kg i.v., fentanyl produced significantly stronger PPT increases than NFEPP in both paws (Fig. 3A). At 32 μg/kg i.v., fentanyl was lethal because of respiratory depression, whereas NFEPP did not elicit overt sedation or respiratory depression but elevated PPT up to 75 g. The most effective

Fig. 2. NFEPP activates MOR-dependent signaling pathways preferentially at low pH in MOR-transfected HEK293 cells. (**A** and **B**) Displacement of bound [^{3}H][D-Ala^2,*N*-Me-Phe^4,Gly^5-ol]-enkephalin (DAMGO) by (A) fentanyl or (B) NFEPP incubated for 90 min at pH 5.5, 6.5, and 7.4. Insets show K_i (n = 6 to 8). (**C** to **F**) $G\alpha_{i1}$-$G\beta_1G\gamma_2$ dissociation detected by FRET efficiency (percentage of initial intensities, corrected for photobleaching) from 20 s before to 140 s after application (dotted lines) of (C and E) fentanyl or (D and F) NFEPP with or without naloxone (NLX) at (C and D) pH 7.4 and (E and F) 6.5. (**G**) Area under the curve (AUC) from (C) to (F) calculated between dotted line and maximal response (upward ticks on x axes) (n = 10). (**H**) IC_{50} of cAMP inhibition at different pH values for fentanyl (open bars) and NFEPP (filled bars) (n = 6). $^{**}P$ < 0.01, $^{***}P$ < 0.001 fentanyl versus NFEPP; $^{###}P$ < 0.001 fentanyl or NFEPP versus fentanyl + NLX or NFEPP + NLX, two-way analysis of variance (ANOVA) and Bonferroni test (means ± SEM).

Corrected 8 June 2017. See Erratum.

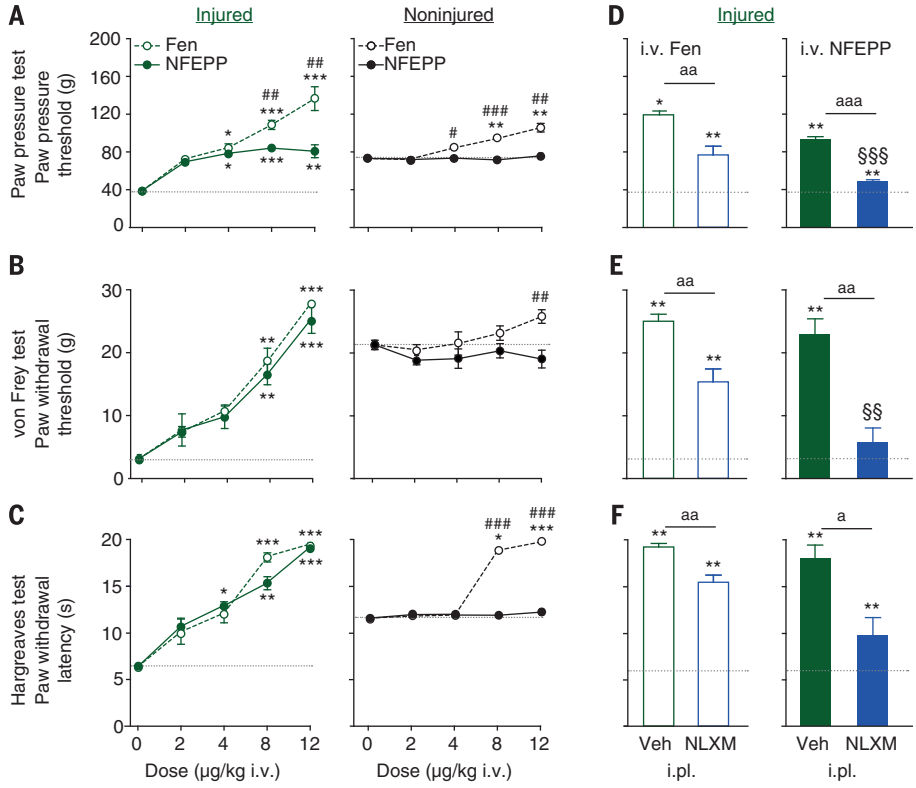

Fig. 3. Systemic NFEPP reduces pain selectively in injured tissue via peripheral MOR in the CFA model. Effects at 10 min after intravenous (i.v.) fentanyl or NFEPP on (**A**) mechanical hyperalgesia, (**B**) allodynia, and (**C**) heat sensitivity in inflamed (left) and noninflamed paws (right). (**D** to **F**) Contribution of peripheral MOR to the analgesia produced 10 min after i.v. injection of fentanyl (left) or NFEPP (right) (each at 12 µg/kg) assessed with naloxone methiodide (NLXM, 50 µg) or vehicle (Veh) injected i.pl. into inflamed paws. $^{\#}P < 0.05$, $^{\#\#}P < 0.01$, $^{\#\#\#}P < 0.001$ fentanyl versus NFEPP, $^{a}P < 0.05$, $^{aa}P < 0.01$, $^{aaa}P < 0.001$ versus NLXM, §§$P < 0.01$, §§§$P < 0.001$ NFEPP + NLXM versus fentanyl + NLXM, Mann-Whitney test (A to F); *$P < 0.05$, **$P < 0.01$, ***$P < 0.001$ versus dotted gray lines, representing "0 µg/kg" in (A) to (C) (Kruskal-Wallis and Dunn's test) or baseline in (D) to (F) (means ± SEM; $n = 6$ to 9).

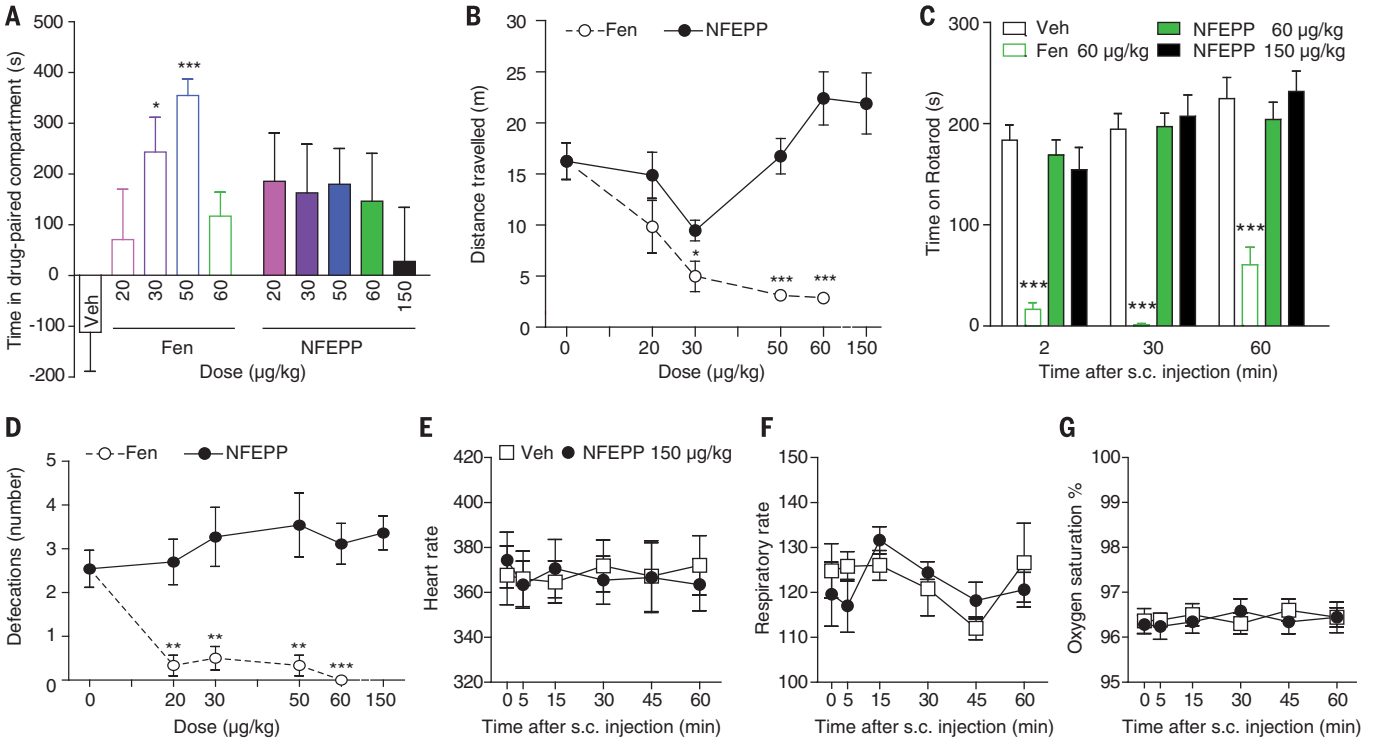

Fig. 4. Systemic NFEPP does not induce central or intestinal side effects. Effect of subcutaneous (s.c.) fentanyl and NFEPP on (**A**) unbiased conditioned place preference, (**B**) locomotor activity expressed as distance travelled during 30 min after drug injection, (**C**) motor coordination measured as time spent on the accelerating Rotarod, (**D**) constipation assessed by number of excreted fecal pellets during 1 hour after drug injection, (**E**) heart rate, (**F**) respiratory rate, and (**G**) blood oxygen saturation. *$P < 0.05$, **$P < 0.01$, ***$P < 0.001$ versus vehicle (0 µg), Kruskal-Wallis and Dunn's test [(A), (B), and (D); $n = 8$ to 12]; two-way related measures ANOVA and Bonferroni test [(C), $n = 8$ to 10); and (E) to (G), $n = 5$] (means ± SEM).

Corrected 8 June 2017. See Erratum.

fentanyl dose (12 μg/kg i.v.) increased PWT and PWL to cut off in both inflamed and contralateral paws (Fig. 3 and fig. S4). NFEPP (12 μg/kg i.v.) also fully restored PWT and PWL, but only in inflamed paws (Fig. 3 and fig. S4).

To examine the contribution of peripheral opioid receptors, we used naloxone-methiodide (NLXM), an opioid antagonist that does not cross the blood-brain barrier (*29*), in optimal doses determined in pilot experiments. In all three tests, the bilateral analgesic effects of fentanyl (12 μg/kg i.v.) were only partially reversed by i.pl. injection of NLXM (50 μg/paw) into inflamed (Fig. 3, D to F) or noninflamed paws (fig. S5). In contrast, the unilateral analgesic effects of NFEPP (12 μg/kg i.v.) in inflamed paws were virtually abolished by NLXM (50 μg/paw i.pl.) (Fig. 3, D to F). In naïve animals, systemic fentanyl (12 μg/kg i.v.) significantly increased PPT in both hindpaws, whereas NFEPP had no effect (fig. S6).

Next, we investigated typical side effects mediated by central opioid receptors (reward, sedation, motor impairment, and respiratory depression) or intestinal opioid receptors (constipation). In the unbiased, conditioned place preference (CPP) paradigm, fentanyl [30 to 50 μg/kg subcutaneously (s.c.)] produced dose-dependent preference (reward) for the drug-associated compartment. As commonly observed in this paradigm (*30*, *31*), this effect decreased at high doses (60 μg/kg s.c.) (Fig. 4A). Conversely, NFEPP (up to 150 μg/kg s.c.) did not show significant effects compared with vehicle (Fig. 4A). Fentanyl (20 to 60 μg/kg s.c.) dose-dependently reduced locomotion, whereas NFEPP (20 to 150 μg/kg s.c.) had no effects (Fig. 4B). Fentanyl (60 μg/kg s.c.) markedly reduced the time to fall off an accelerating Rotarod compared with vehicle or NFEPP (60 to 150 μg/kg s.c.) (Fig. 4C). Compared with controls, fentanyl (20 to 60 μg/kg s.c.) significantly reduced defecation, whereas NFEPP (20 to 150 μg/kg s.c.) had no effect (Fig. 4D). Heart rate, respiratory rate, and blood oxygen saturation were indistinguishable between NFEPP (150 μg/kg s.c.) and vehicle (Fig. 4, E to G).

Previous strategies to improve analgesics have failed to yield drugs without side effects (*1*–*6*, *11*, *25*, *32*). In contrast to other targets (e.g., blockade of individual excitatory ion channels or receptors on sensory neurons) (*6*), the advantages of peripheral opioid receptor activation include reduced tolerance and the synergistic modulation of multiple ion currents (*11*) implying a wider range of efficacy. Therefore, we exploited injury-specific MOR-ligand interactions at low pH. By combining quantum-chemical simulations with classical modeling, we demonstrated the importance of protonation for receptor binding and activation (*5*, *20*), and we designed a new ligand with low pK_a and decreased receptor affinity at physiological pH. Consistently, NFEPP induced G-protein dissociation only at low pH, and its potency of cAMP inhibition decreased with increasing extracellular pH. In contrast, receptor binding and activation by fentanyl did not change, likely because of its similar protonation status under all pH conditions.

In two animal models of painful inflammation with decreased tissue pH (reflecting 2.5- and 1.6-fold increased proton concentrations, respectively), NFEPP did not act in healthy central or peripheral compartments but produced analgesia by selective activation of peripheral MOR in injured tissue, i.e., at the source of pain generation. Note that NFEPP did not produce reward, sedation, motor impairment, respiratory depression, or constipation. Targeting "disease-specific" (i.e., pathological rather than physiological) conformations of receptors and ligands represents a paradigm shift in drug design. This yielded a novel opioid analgesic of similar efficacy to conventional fentanyl, however, devoid of detrimental side effects.

REFERENCES AND NOTES

1. V. J. Dzau, P. A. Pizzo, *JAMA* **312**, 1507–1508 (2014).
2. N. Bhala *et al.*, *Lancet* **382**, 769–779 (2013).
3. R. M. Califf, J. Woodcock, S. Ostroff, *N. Engl. J. Med.* **374**, 1480–1485 (2016).
4. I. D. Pogozheva, M. J. Przydzial, H. I. Mosberg, *AAPS J.* **7**, E434–E448 (2005).
5. L. Dosen-Micovic, M. Ivanovic, V. Micovic, *Bioorg. Med. Chem.* **14**, 2887–2895 (2006).
6. N. Richards, S. B. McMahon, *Br. J. Anaesth.* **111**, 46–51 (2013).
7. R. Baron, G. Hans, A. H. Dickenson, *Ann. Neurol.* **74**, 630–636 (2013).
8. J. Sawynok, J. Liu, *Eur. J. Pharmacol.* **734**, 114–121 (2014).
9. I. Tabas, C. K. Glass, *Science* **339**, 166–172 (2013).
10. P. Holzer, *Handb. Exp. Pharmacol.* **194**, 283–332 (2009).
11. C. Stein, *Annu. Rev. Med.* **67**, 433–451 (2016).
12. C. Jagla, P. Martus, C. Stein, *Pain* **155**, 2056–2062 (2014).
13. C. Gaveriaux-Ruff *et al.*, *Pain* **152**, 1238–1248 (2011).
14. R. Weibel *et al.*, *PLOS ONE* **8**, e74706 (2013).
15. S. R. Childers, *J. Neurochem.* **50**, 543–553 (1988).
16. M. G. Ludwig *et al.*, *Nature* **425**, 93–98 (2003).
17. X. Deupi, B. K. Kobilka, *Physiology (Bethesda)* **25**, 293–303 (2010).
18. K. P. Hofmann *et al.*, *Trends Biochem. Sci.* **34**, 540–552 (2009).
19. L. Ye, N. Van Eps, M. Zimmer, O. P. Ernst, R. S. Prosser, *Nature* **533**, 265–268 (2016).
20. J. G. Li *et al.*, *Life Sci.* **65**, 175–185 (1999).
21. W. Huang *et al.*, *Nature* **524**, 315–321 (2015).
22. R. Sounier *et al.*, *Nature* **524**, 375–378 (2015).
23. A. Manglik *et al.*, *Nature* **485**, 321–326 (2012).
24. M. A. Schumacher, A. I. Basbaum, W. L. Way, in *Basic and Clinical Pharmacology*, B. G. Katzung, S. B. Masters, A. J. Trevor, Eds. (McGraw-Hill Medical, New York, 2009), pp. 531–552.
25. M. Filizola, H. O. Villar, G. H. Loew, *J. Comput. Aided Mol. Des.* **15**, 297–307 (2001).
26. J. R. Deschamps, J. L. Flippen-Anderson, C. George, *Biopolymers* **66**, 287–293 (2002).
27. R. L. Thurlkill, D. A. Cross, J. M. Scholtz, C. N. Pace, *J. Cardiothorac. Vasc. Anesth.* **19**, 759–762 (2005).
28. S. D. Roy, G. L. Flynn, *Pharm. Res.* **6**, 147–151 (1989).
29. D. R. Brown, L. I. Goldberg, *Neuropharmacology* **24**, 181–191 (1985).
30. S. Karimi, M. Karami, H. Zardooz, S. H. Salimi, H. Sahraei, *Iran. J. Pharm. Res.* **10**, 605–610 (2011).
31. C. Canestrelli, N. Marie, F. Noble, *Int. J. Neuropsychopharmacol.* **17**, 1367–1373 (2014).
32. E. R. Viscusi *et al.*, *Pain* **157**, 264–272 (2016).

ACKNOWLEDGMENTS

This work was supported by Bundesministerium für Bildung und Forschung (VIP 0272/03V0364). We thank H. Schick and C. Wedler (ASCA GmbH) for continuous consulting, N. Vogel for technical assistance, M. Adjobo-Hermans for helpful advice and for donating the Venus-$G\gamma_2$ construct, O. Perepelica for initial computational simulations, P. Deuflhard and C. Zöllner for stimulating discussions, and B. Kieffer for critical comments on the manuscript. The Charité-Universitätsmedizin Berlin and the Zuse Institute Berlin have filed a patent on pH-dependent opioid receptor agonists (US 9133120 B2). A patent application on the computational methods (PCT/EP2013/102681) is pending. All data can be accessed at www.zib.de/ext-data/selective-opioids/.

SUPPLEMENTARY MATERIALS

www.sciencemag.org/content/355/6328/966/suppl/DC1
Materials and Methods
Supplementary Text
Figs. S1 to S10
Table S1
References (*33*–*67*)

24 August 2016; accepted 30 January 2017
10.1126/science.aai8636

A nontoxic pain killer designed by modeling of pathological receptor conformations

V. Spahn, G. Del Vecchio, D. Labuz, A. Rodriguez-Gaztelumendi, N. Massaly, J. Temp, V. Durmaz, P. Sabri, M. Reidelbach, H. Machelska, M. Weber and C. Stein

Science **355** (6328), 966-969.
DOI: 10.1126/science.aai8636

A pain killer without side effects

Opioids are very strong and effective pain killers. However, they also have a range of well-known side effects and can cause addiction. Painful conditions such as inflammation or trauma are often associated with localized tissue acidification. Spahn *et al.* designed a novel opioid receptor agonist that, unlike clinically used opioids, best activates the receptors in such acidified tissues. In rat models of inflammatory pain, the new drug exerted strong pain relief essentially without the side effects of standard opioids.

Science, this issue p. 966

Revised 29 June 2017; see below

www.sciencemag.org/content/355/6328/966/suppl/DC1

Supplementary Materials for

A nontoxic pain killer designed by modeling of pathological receptor conformations

V. Spahn,* G. Del Vecchio,* D. Labuz, A. Rodriguez-Gaztelumendi, N. Massaly, J. Temp, V. Durmaz, P. Sabri, M. Reidelbach, H. Machelska, M. Weber,† C. Stein†‡

*These authors contributed equally to this work.
†These authors contributed equally to this work.
‡Corresponding author. Email: christoph.stein@charite.de

Published 3 March 2017, *Science* **355**, 966 (2017)
DOI: 10.1126/science.aai8636

This PDF file includes

Revised 29 June 2017: In this revision (shown in red characters), text has been added to describe the synthesis and characterization of NFEPP, and three figures have been added to show the structural and physical characteristics and spectra of NFEPP. The conclusions of the Report remain unchanged. The originally posted supplementary materials are available here.

Materials and Methods

Quantum mechanical pK_a calculations

For the estimation of pK_a values we used *Gaussian 09* and the quantum-chemical method proposed previously (*33, 34*). To predict the Gibbs free energy change associated with deprotonation in water, the geometries of protonated and deprotonated molecules were fully optimized by employing density functional theory using Becke's three-parameter hybrid exchange functional and the Lee-Yang-Parr correlation functional (B3LYP) with the 6-31+G* basis set. Harmonic vibrational frequencies were then determined at the same level (B3LYP/6-31+G*) to evaluate the thermal corrections to the Gibbs free energy at T = 298.15 K. The "integral equation formulation of the polarizable continuum model" was used in solvation calculations on protonated and deprotonated states of molecular species to evaluate their free energies in aqueous solution. All solvation optimizations were performed at the HF/6-31+G* level (by the Hartree Fock method) using the geometries optimized at the B3LYP/6-31+G* level in the gas phase.

Classical binding free energy calculations

For derivatives and promising candidates estimations of Gibbs free energies of binding were carried out by classical molecular dynamics (MD) simulations with Groningen Machine for Chemical Simulations (GROMACS). These small molecules were sketched, cleaned in 3D, and exported to the pdb file format using the program *MarvinSketch v5.5*. Physical parameters were assigned according to the General AMBER Force Field (GAFF) (*35*) with the aid of the AmberTool Antechamber (*36, 37*). Partial atomic charges were calculated using the AM1BCC method (*38*). The most recent structural entry (*21*) of available X-ray crystallographic MOR files from the Protein Data Bank (PDB, entry "5C1M") obtained hydrogen patterns specific for pH 5 and physiological pH. A few single amino acid atoms were missing and assigned with the aid of DeepView (Swiss-PdbViewer) v4.1 (*39*) followed by a parametrization according to the Amber99sb-ildn (*40*) force field. As described recently in (*41*), 60 uniformly distributed initial orientations of each ligand were constructed at both respective proteins' binding sites replacing the co-crystallized ligand of PDB:5C1M with respect to their geometric centers. An additional starting configuration included the unbound ligand only. Having explicitly solved each of these systems with the TIP4PEW model (*42*) in a simulation box of 10 nm edge length and neutralized formal charges using sodium and chlorine ions, they underwent 4 major simulation steps with GROMACS v.5.1.1 (*43*): (i) at most, 7000 steepest descent energy minimization steps if the maximum force acting on any atom had not ended up below 150 kJ mol^{-1} nm^{-1} before; (ii) 100 ps temperature equilibration MD (NVT ensemble) with position restraints on complex atoms; (iii) 300 ps of pressure equilibration MD (NPT ensemble) without position restraints; and (iv) 400-ps production run with slight position restraints on backbone atoms (GROMACS mass factor 50). During the production run, the temperature and pressure were coupled to 310 K and 1 bar by velocity rescaling (*44*) and according to the Parrinello-Rahman method (*45*), respectively. Due to LINCS constraints (*46*), the integration step size was increased to 2 fs. The smooth particle mesh Ewald summation (*47*) was used for the calculation of Coulomb potentials. A collection of 1000 snapshots associated with 0.2-ps time offsets were made for analysis. Differences of Gibbs free energies of binding ΔG in kJ mol^{-1} between the bound and unbound system were then estimated for each of the 60 binding

modes as described by Åqvist et al. (*48*) and by using the suggested coefficients 0.5 and 0.162 for averages associated with the two force field interaction energy contributions which are related to electric and van der Waals forces, respectively. For each ligand, the binding mode associated with the lowest ΔG value and, thus, with the highest statistical weight is listed in Table S1.

Chemicals and Drugs

Fentanyl citrate (F3886), naloxone hydrochloride (NLX; N7758), naloxone methiodide (NLXM), D-Phe-Cys-Tyr-D-Trp-Orn-Thr-Pen-Thr-NH_2 (CTOP), 17,17′-(dicyclopropylmethyl)-6,6′,7,7′-6,6′-imino- 7,7′-binorphinan-3,4′,14,14′-tetrol dihydrochloride (norBNI) were purchased from Sigma-Aldrich (Taufkirchen, Germany), [^{3}H][D-Ala^2,*N*-Me-Phe^4,Gly^5-ol]-enkephalin (DAMGO) from Perkin Elmer (Waltham, USA), and [allyl]2-Tyr-α-amino-isobutyric acid (Aib)-Aib-Phe-Leu-OH (ICI 174,864) from Biozol (Eching, Germany). (±)-*N*-(3-fluoro-1-phenethylpiperidine-4-yl)-*N*-phenylpropionamide (NFEPP) was synthesized according to our design by a contractor (ASCA GmbH, Berlin, Germany), as described in detail in the next section. For *in vivo* experiments, NFEPP was dissolved in dimethyl-sulfoxide (DMSO) and diluted with 0.9% NaCl to obtain the final concentrations (maximum DMSO: 4.2% for subcutaneous (s.c.) or up to 0.5% for intravenous (i.v.), and intraplantar (i.pl.) injections. Fentanyl and opioid receptor antagonists were dissolved in 0.9% NaCl. Control groups were treated with DMSO or NaCl, respectively. For *in vitro* experiments, fentanyl and NFEPP were initially dissolved in DMSO and diluted in assay buffer to final concentrations. The experimental measurement of the pK_a value of NFEPP was performed by a contractor (Sirius Analytical Ltd., Forest Row, UK).

NFEPP synthesis

Step 1: Production of a silyl enol ether

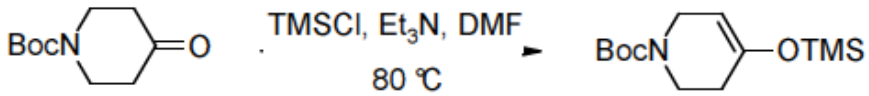

199.25 g/mol 271.44 g/mol

The reactant (3 g; 15.056 mmol; 1 eq) was dissolved in dry dimethylformamide under argon and was subsequently mixed first with triethylamine (1953 mg; 18.079 mmol; 2.4 eq) and thereafter with chlortrimethylsilane (5 ml; 36.134 mmol; 1.2 eq). The reaction ran for 16 hours at 80°C. The reaction mixture was transferred to a separating funnel with cyclohexane (100 ml) and washed 3 times with sodium hydrogen carbonate solution (3 × 40 ml). After drying over magnesium sulfate and concentrating under vacuum, the product was rinsed 4 times with toluene to completely remove the dimethylformamide. A yellow-brown oil was obtained.

Step 2: Fluorination

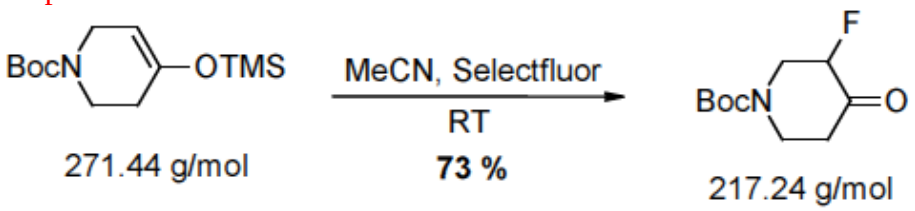

The raw product from step 1 (2,566 mg; 9.453 mmol; 1 eq) was dissolved under argon in dry acetonitrile and mixed with 1-chloromethyl-4-fluoro-1,4-diazoniabicyclo[2.2.2]octane bis(tetrafluoroborate) (3,681 mg; 10.397 mmol; 1.1 eq) (Selectfluor, a commercially available fluorine donor). After 60 min shaking at room temperature, the mixture was transferred with ethylacetate (250 ml) to a separating funnel and washed first with diluted (2 × 75 ml) and afterwards with saturated NaCl solution (80 ml). The organic phase was dried over magnesium sulfate and subsequently concentrated under vacuum. The obtained product was clean without requiring any further purification steps. A light brown resin was obtained.

Step 3: Reductive amination

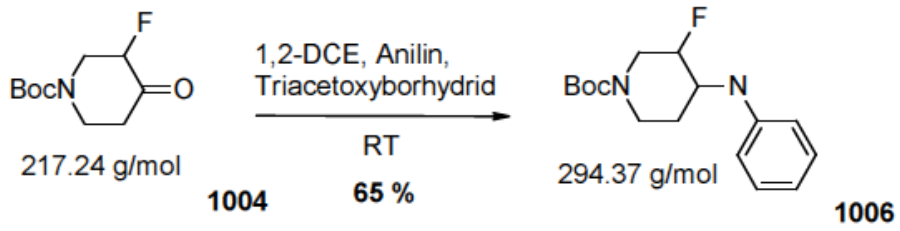

The fluorinated compound (1,410 mg; 6.491 mmol; 1 eq) was presented with aniline (0.65 ml; 7.140 mmol; 1.1 eq) and sodium triacetoxyborhydride (2,064 mg; 9.737 mmol; 1.5 eq), and dissolved under argon in dry 1,2-dichloroethane. The reaction took 18 h at room temperature. The reaction mixture was transferred with sodium hydrogen carbonate solution (70 ml) to a separating funnel and extracted with ethylacetate (2 × 70 ml). The combined organic phases were dried over magnesium sulfate and concentrated. Subsequently, the product was purified by column chromatography [silica gel 60; cyclohexane/ethylacetate 19:1 (1,500 ml), 15:1 (800 ml), 10:1 (2,200 ml)]. A colorless solid product was obtained.

Step 4: Removal of the protecting group

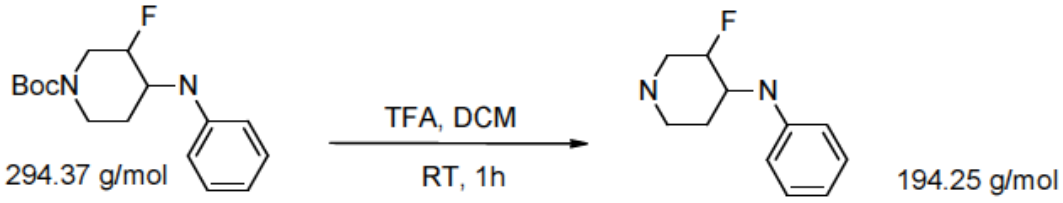

The product (824 mg; 2.799 mmol; 1 eq) was dissolved in a mixture of dichloromethane and trifluoroacetic acid (2:1, 9 ml) and shaken for 1 h at room temperature. Subsequently all liquid was removed under vacuum and a brown oil was obtained. The oil was transferred with methanol (2 × 20 ml) to a separating funnel. Distilled water (40 ml), 5 N caustic soda (8 ml) and saturated sodium chloride solution (30 ml) were added.

Subsequently the product was extracted with ethylacetate (2 × 100 ml). Water and diethyl ether were added until a phase separation occurred. The combined organic phases were dried over magnesium sulfate and subsequently dried under vacuum. A brown resin was obtained.

Step 5: Alkylation

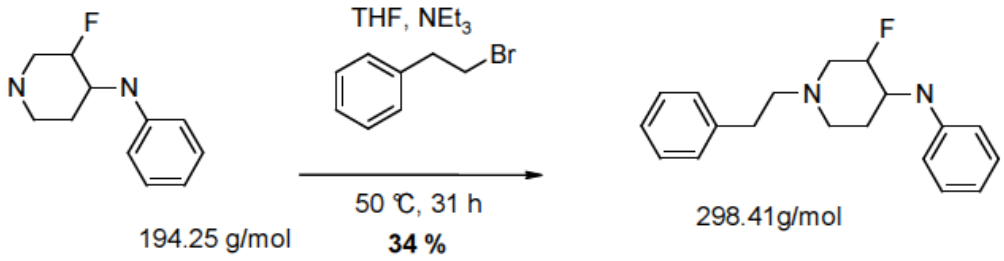

The resin (1,198 mg; 6.167 mmol; 1 eq) was dissolved under argon in dry tetrahydrofuran (80 ml). Subsequently, triethylamine (1.71 ml; 12.335 mmol; 2 eq) and phenethylbromide (2.50 ml; 18.501 ml; 3 eq) were added. The reaction took 30 h at 50°C. Afterwards the reaction mixture was transferred with ethylacetate (250 ml) to a separating funnel and washed with sodium hydrogen carbonate solution (2 × 100 ml). The organic phase was dried over magnesium sulfate, concentrated under vacuum, and a brown oil was obtained. The product was purified by column chromatography [silica gel 60; cyclohexane/ethylacetate 10:1 (1,320 ml), 5:1 (300 ml), 3:1 (2,100 ml)]. After purification, a colorless solid product was obtained.

Step 6: Acylation

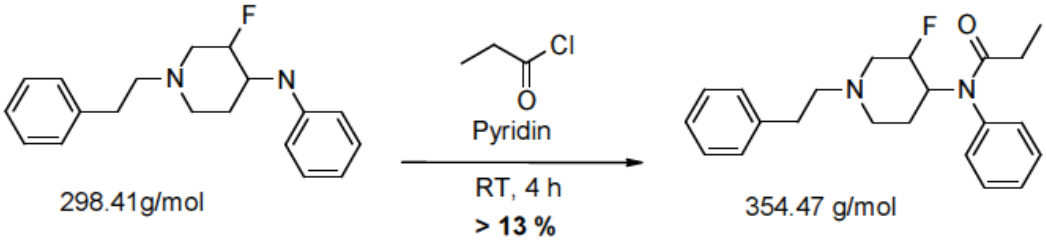

The product (661 mg; 2.215 mmol; 1 eq) was dissolved in pyridine (35 ml) and, while shaking, mixed with propionylchloride (0.59 ml; 6.756 mmol; 3 eq). The reaction took 4 h at room temperature. Subsequently, the reaction mixture was transferred with chloroform (2 × 50 ml) to a separating funnel and washed with distilled water (60 ml). A colorless solid product precipitated which was separated with a frit and discarded. The organic phase was again washed with distilled water (50 ml). The product was purified by column chromatography [silica gel 60; cyclohexane/ethylacetate 4:1 (2,650 ml), 3:1 (800 ml), 1:1 (400 ml), ethylacetate (250 ml)]. The fractions, which only contained product, were concentrated, and a yellow oil was obtained. The oil was resuspended in diethylether and, by addition of *n*-pentane, a light yellow solid product was precipitated. The contractor (ASCA GmbH) performed several proprietary separation procedures at different steps throughout this synthesis. The major diastereomer was isolated at nearly 100 % purity, as shown by ^{1}H- and ^{19}F-NMR (fig. S12), and used in our *in vitro* and *in vivo* experiments.

Cell cultures

As described previously (*49*), MOR-expressing or wild-type human embryonic kidney 293 (HEK293) cells were maintained in DMEM media supplemented with fetal bovine serum, 100 U/ml penicillin and 100 µg/ml streptomycin with or without 0.1 mg/ml geneticin, respectively, in 5% CO_2 at 37°C. Cells were passaged 1:3–1:10 every second to third day from P8 to P28 depending on confluence.

Radioligand binding assay

HEK293 cells stably expressing rat MOR were cultured in flasks with a growth area of 175 cm². Cells were washed with ice-cold Trizma (50 mM, pH 7.4), scratched with a cell scraper, homogenized and centrifuged twice at 42,000*g* for 20 min at 4°C as described previously (*49-51*). Protein concentration was determined using the Bradford method (*52*). The corrected half maximal concentration (IC_{50}) of fentanyl or NFEPP required to displace 4 nM of the standard MOR ligand [^{3}H]DAMGO from the receptor was determined at different pH values (5.5, 6.5, 7.4). A protein amount of 80-100 µg was incubated with [^{3}H]DAMGO (50 Ci/mmol) and the competing ligands (fentanyl or NFEPP) were dissolved in 50 mM Trizma at pH 7.4 for 15, 30, or 90 min (to investigate differing binding kinetics) at room temperature. Nonspecific binding was determined by the addition of 10 µM NLX. Saturation-binding with [^{3}H]DAMGO was performed to determine its affinity at pH 5.5, 6.5 and 7.4. A protein amount of 100 µg was incubated with 0.5, 1, 2, 4, 8 and 16 nM [^{3}H]DAMGO (51 Ci/mmol) for 90 min at room temperature. K_D of [^{3}H]DAMGO was calculated using non-linear regression curve fit. K_i was calculated according to Cheng-Prusoff (see Data handling and statistical analyses). Filters were soaked in 0.1% polyethyleneimine solution before use. Bound and free ligands were separated by rapid filtration under vacuum through Whatman GF/B glass fiber filters. Bound radioactivity was determined by liquid scintillation spectrophotometry at 69% counting efficiency for [^{3}H] after overnight extraction of the filters in scintillation fluid.

Transfection, constructs and site-directed mutagenesis for FRET experiments

Confluent wild-type HEK293 cells (70–90%) were plated on 30 mm diameter plastic culture dishes coated with poly-L-lysine 24 h before transfection. Transfection of 0.3–1 µg cDNA per construct was performed using X-treme GENE HP DNA reagent following the supplier's recommendations. The plasmid containing the cDNA encoding the FLAG-epitope-tagged rat MOR (oprm1, NM_013071.2) in pcDNA™3.1 vector with geneticin resistance gene was provided by Prof. Christian Zöllner (University Hamburg, Germany). To preserve the essential role of amino and carboxyl termini of Gα subunits for plasma membrane localization and heterotrimerization with Gβγ subunits, fluorescent $G\alpha_{i1}$ was obtained by inserting enhanced cyan fluorescent monomeric Turquoise (mTq) within the αb-αc loop between residues 121 and 122 based on previous studies using similar insertions with $G\alpha_i$ (*53-56*), $G\alpha_s$ (*57*) or $G\alpha_q$ (*58*). Furthermore, the last six amino acids of the Tq protein ($G\alpha_{i1}$mTqΔ6) were deleted, which was previously suggested to force the fluorophore into a FRET-promoting orientation (*57*). Rat $G\alpha_{i1}$ (Gnai1, NM_013145.1), labeled with truncated mTq ($G\alpha_{i1}$–mTqΔ6) (*58*), and TC-epitope-tagged-$G\beta_1$ (Gnb1, NM_030987.2) were cloned into vectors and were subsequently subcloned into pcDNA™3.1 expression vector between BamH1 or EcoRI and XhoI, respectively. A human construct with circular permutated Venus-$G\gamma_2$ was kindly provided by Dr.

Adjobo-Hermans (Radboud University Nijmegen Medical Centre, The Netherlands). The rat variant of Venus-$G\gamma_2$ (Gng2, NM_001257349.1) and the PTX-resistant $G\alpha_{i1}$-mTqΔ6 were generated by mutagenesis (N24S and C351I, respectively) using QuikChange™ Mutagenesis kit, and then checked by sequencing. Because the insertion of fluorescent residues may impede Gα-effector interactions (*54*), the functionality of the transfected G-protein subunits was confirmed by demonstrating intact cAMP inhibition by fentanyl in the presence of PTX.

Real-time FRET measurements

At 48–72 h after transfection of HEK293 cells with MOR, $G\beta_1$, $G\alpha_{i1}$-mTqΔ6 and Venus-$G\gamma_2$, FRET between the latter two proteins was measured. Cells were briefly washed with PBS and subsequently equilibrated with assay buffer (140 mM NaCl, 5 mM KCl,2 mM $CaCl_2$,2 mM $MgCl_2$, 10 mM HEPES, 10 mM Glucose) at different pH values. We used a FRET Nikon Eclipse TE2000-S widefield microscope equipped with a ultra-high-quality monochrome camera DS-Qi1, a Polychrome V monochromator and a DualView beam splitter to separate yellow fluorescent protein (YFP) (535 ± 15 nm) and cyan fluorescent protein (CFP) (480 ± 20 nm) emissions. Images of donor-donor (DD; excitation 439 nm/emission 480 nm), donor-acceptor (DA; excitation 439 nm/emission 535 nm) and acceptor-acceptor (AA; excitation 505 nm/emission 535 nm) were taken with a 40X objective (S fluor/1.30 oil) every 500 ms with exposure times kept constant and comprised between 50 (for Venus) and 150 ms (for mTq). Fluorescence intensities were quantified on regions of interest (ROI) including the whole cell by NIS-Elements software. After subtraction of background, NIS-Elements calculated FRET efficiency (in%), taking into account bleed-through and direct Venus excitation (*59, 60*). Preliminary experiments with cells expressing only mTq or Venus were performed to calculate the correction coefficients for the acceptor chromophore (CoA) and for the donor chromophore (CoB), accounting for bleed-through and direct YFP excitation from 3 independent experiments (CoA = 0.19; CoB = 0.43). On the day of the experiment, cells were washed and incubated with assay buffer (at pH 7.4 or 6.5) and after 20 s of live imaging, fentanyl or NFEPP were added at a final concentration of 100 µM (in 0.1% DMSO) for the remaining time. The concentration was based on preliminary dose-response experiments with fentanyl (fig. S2K). In antagonist experiments, NLX was administered together with agonists at a final concentration of 1 mM. For each ROI, background-corrected fluorescence intensities and corresponding FRET parameters (FRET efficiency > 0.5%) over time were normalized to initial values (= 1), pooled by experiment and finally averaged across the experiments. For net AUC calculation, net FRET% for each treatment group was derived by subtraction of vehicle-treated FRET%.

cAMP accumulation

MOR-expressing HEK293 cells were cultivated in a 96-well-plate and incubated with 10 µM forskolin (FSK) and 2 mM of the phosphodiesterase inhibitor 3-Isobutyl-1-methyl-Xanthin (IBMX) for 20 min in the absence or presence of different concentrations of fentanyl or NFEPP under different pH conditions (5.5–7.4) in the absence or presence of NLX (10 µM). Treatment with FSK/IBMX induces adenylyl cyclase activity and precludes cAMP degradation, respectively (*61*). cAMP measurements were performed using the cAMP Biotrak Enzymeimmunoassay and an ELISA-photometer at 450 nm according to the manufacturer's instructions.

Animals

All protocols were approved by the State animal care committee (Landesamt für Gesundheit und Soziales, Berlin). Male Wistar rats (200–300 g) were kept on a 12 h light/dark schedule with food and water *ad libitum*. Room temperature was 22 ± 0.5 °C and humidity was 60–65%. Statistical power calculations were performed *a priori* to minimize the number of animals. Rats were handled once per day for 1-2 min (before nociceptive testing) or habituated to the test cages (1-2 times for 15 min), starting 4 days prior to experiments. After completion of experiments, animals were killed with isoflurane.

Paw inflammation with complete Freund's adjuvant (CFA)

Rats received an i.pl. injection of CFA (150 µl) into the right hindpaw under brief isoflurane anesthesia (*62*). Experiments were performed 4 days thereafter.

Paw incision

Unilateral hindpaw incision was performed under isoflurane anesthesia as described elsewhere (*63*). Briefly, a 1 cm longitudinal incision was made with a No. 11 blade through skin and fascia of the plantar aspect of the paw, starting 0.5 cm from the proximal edge of the heel and extending towards the toes. The plantaris muscle was elevated and incised longitudinally. The muscle origin and insertion remained intact. The wound was closed with silk sutures. Experiments were performed 2 hours thereafter.

In vivo pH measurement

A pH-sensitive glass microelectrode was calibrated using reference solutions of pH 4.0, 7.0 and 9.2. Rats were anesthetized with isoflurane. A 20-gauge needle was used to pierce the plantar skin of the hindpaws. The microelectrode mounted in the lumen of a 20-gauge needle was advanced 3- to 6-mm deep into the paw tissue. Stable readings were obtained 2-3 min after insertion.

Injections

I.v. (200 µl) and i.pl. (100 µl) injections were performed under brief isoflurane anesthesia. The experimenter was blinded to the treatments/doses. Effects on nociceptive thresholds were evaluated in separate groups of animals, before and 5–60 min following injections of agonists. NLXM was co-injected i.pl. with agonists or injected i.pl. immediately before i.v. injection of agonists. CTOP, ICI 174,864 and norBNI were co-injected i.pl. with agonists. Pain thresholds were measured 5 or 10 min after i.pl. or i.v. injections, respectively. For assessment of side effects, injections were performed s.c. without anesthesia. All dosages were determined in pilot experiments.

Mechanical hyperalgesia (Randall-Selitto test)

Rats were gently restrained under paper wadding and incremental pressure was applied via a wedge-shaped, blunt piston onto the dorsal surface of the hindpaws by means of an automated gauge. The paw pressure threshold (PPT; cut-off at 250 g) required to elicit paw withdrawal was determined by averaging three consecutive trials separated by 15-s intervals. The sequence of paws was alternated between animals to avoid "order" effects.

Mechanical allodynia (von Frey test)

Animals were individually placed in clear Plexiglas cubicles located on a stand with anodized mesh. The plantar surface of each hindpaw was stimulated with von Frey filaments of increasing force until the filament that produced withdrawal responses to 3 stimuli (paw withdrawal threshold; PWT) was reached as described previously (*64*). Von Frey filaments were 0.6, 1, 1.4, 2, 4, 6, 8, 10, 15 and 26 g.

Heat hypersensitivity (Hargreaves test)

Rats were individually placed in clear Plexiglas cubicles positioned on a stand with glass surface. Radiant heat generated by a high-intensity light bulb was applied to the plantar surface of the hindpaws from underneath the glass surface, and paw withdrawal latency (PWL) was measured using an electronic timer as described (*65*). Three measurements separated by at least 10 s were averaged. The heat intensity was adjusted to obtain a baseline (BL) withdrawal latency of about 10–12 s in uninjured paws, and the cut-off was 20 s.

Conditioned Place Preference (CPP)

We used an unbiased counterbalanced CPP protocol as described elsewhere (*66, 67*). Briefly, light- and sound-attenuating chambers (60 × 30 × 30 cm) consisted of two compartments separated by a removable door. The two compartments differed in wall color (black or white with black stripes) and floor texture ("grid" or "hole"). For habituation, each naïve rat was placed into the CPP apparatus (without separator) and was allowed to freely explore it for 30 min (days 1 and 2). For the pre-conditioning test, each rat was placed into the CPP apparatus (without separator) for 15 min and the time spent in each compartment was recorded (day 3). If rats showed high unconditioned preference for one of the two compartments in this phase, they were excluded from further analysis (ca. 10% of animals). During conditioning, treatment and treatment-associated compartment were assigned randomly. Each rat underwent three 60 min conditioning sessions receiving the test substance in one compartment (one session every other day), and three 60 min sessions receiving vehicle in the other compartment on the alternate days (days 4–9). On the test day (day 10), no drug was administered and each rat was allowed to freely explore the entire CPP apparatus (without separator) for 15 min. The time spent in each compartment was recorded using the AnyMaze software. Preference was calculated as time spent in drug compartment minus time spent in the vehicle compartment.

Locomotor activity

On the first day of conditioning (day 4), naïve animals' horizontal locomotor activity and location in CPP boxes was monitored by an infrared camera using AnyMaze software. Locomotion was measured as the distance (in m) traveled in 5 min intervals during the conditioning session (60 min) following drug administration.

Motor coordination (rotarod test)

Healthy rats were trained on the rotarod for one day at 5 rotations per minute (rpm), and for two days at 10 rpm until they were able to stay on the rotarod for 300 s (maximum 5 trials). Data were then recorded for three baseline trials before drug

exposure, followed by three trials at 2, 30 and 60 min after drug injection at an accelerating speed (10–35 rpm over 300 s). The latency to fall was recorded for 3 successive attempts and averaged for each trial.

Respiratory depression and heart rate

A pulse oximeter was used to measure heart rate, respiratory rate and blood O_2 saturation in accordance with manufacturer's instructions. After 2 days of handling and another 2 days of habituation (30 min/session), naïve rats were placed in a Plexiglass box wearing a pulse oximeter clip (collar clip) around the neck to measure two representative, error-free data sets, which were averaged at each time point post s.c. injections.

Defecation

The excreted fecal pellets of individual naïve rats were counted after 60 min of first drug administration on the first day of conditioning in the CPP boxes.

Data handling and statistical analyses

All data were assessed for normal distribution and equal variances by Kolmogorov-Smirnov or Shapiro-Wilk normality tests. In dose-response experiments (displacement binding and cAMP), means of values at each agonist concentration and each pH were calculated and used to derive EC_{50} and IC_{50} by nonlinear regression and were then subjected to two-way analysis of variance (ANOVA) followed by Bonferroni post-hoc tests, or to Kruskal-Wallis one-way ANOVA followed by Dunn's post-hoc tests. In binding experiments IC_{50} was corrected according to Cheng-Prusoff: $K_i = IC_{50}/([A]/EC_{50} + 1)$ to obtain pH-independent K_i. In FRET experiments, background-corrected fluorescence intensities and corresponding FRET parameters (FRET efficiency > 0.5%) for each ROI were normalized to initial values (= 1), pooled by experiment and finally averaged across the experiments. For net AUC calculation, net FRET% for each treatment group was derived by subtraction of vehicle-treated FRET%. Multiple comparisons were evaluated with two-way ANOVA followed by Bonferroni test for normally distributed data and comparisons between two groups were made using Wilcoxon matched paired test for non-normally distributed data. Behavioral data were expressed as raw values. Two-sample comparisons were made using paired or unpaired *t* test for normally distributed data, or Wilcoxon or Mann-Whitney test for non-normally distributed data. Changes over time (more than two time points) were evaluated using one-way repeated measurements (RM)-ANOVA followed by Bonferroni test for normally distributed data, or Friedman one-way RM-ANOVA followed by Dunn's test for non-normally distributed data, to examine one treatment. Two-way RM-ANOVA and Bonferroni test were used to compare two parameters over time. Multiple comparisons at one time point were performed using one-way ANOVA followed by Bonferroni test for normally distributed data, or Kruskal-Wallis one-way ANOVA followed by Dunn's test for non-normally distributed data. Dose-response relationships were analyzed by linear regression or by nonlinear regression and fitting with the least-squares method. Differences were considered significant if $P < 0.05$. Prism 5 (GraphPad, San Diego, USA) was used for all tests and graphs and all data were expressed as means ± standard error of the mean (SEM).

Supplementary Text

Computer simulations

In computational simulations we integrated structural data on MOR (*21*) and its ligand fentanyl (*25, 26*). We simulated the replacement of hydrogens (Fig. 1A) by fluorine (F), which attracts protons and decreases pK_a. As an additional criterion for selection of suitable candidates we calculated the Gibbs free energy (ΔG) of protonated and deprotonated ligands, derived from classical molecular dynamics (MD) simulations. Low (preferably negative) values of ΔG are associated with high binding affinities. The highest affinities (-16.3 to -20.1 kJ/mol) were found for the protonated derivatives F3* (H-F3, H-F4, H-F6, H-F7) under injured (acidic) conditions (Table S1), as compared to their affinities under noninjured (neutral) conditions (Table S1, italics) or to their nonprotonated forms (F3, F4, F6, F7) under noninjured conditions (Table S1). Using both criteria together, the most promising candidates were H-F3 and H-F7 (Fig. 1C and Table S1). Of note, the binding affinity of protonated fentanyl (H-Fen, negative ΔG) is higher than that of its deprotonated form (Fen, positive ΔG) (Table S1), consistent with our starting point. Also, the protonated N-group is in clear vicinity (5.0 Å) to the side chain oxygens of Asp147, a crucial prerequisite for the binding process (*20*).

Structural and physical characteristics of NFEPP

The synthesized compound had a formula of $C_{22}H_{27}FN_2O$, with a molecular weight of 354.47 g/mol and melting temperature of 110-114 °C. High pressure liquid chromatography coupled with mass spectrometry (HPLC/MS) was employed with the exclusive purpose of determining the mass of the compound (fig. S11). The structure was identified by NMR spectra (fig. S12). Heteronuclear multiple bond correlation (HMBC), heteronuclear single quantum correlation (HSQC) and correlation spectroscopy (COSY) NMR spectra were also obtained (fig. S13). Because the proton coupling constants between the protons at C2 – C3 and C3 - C4 of NFEPP are below 2 Hz, the proton at C3 is equatorial and the proton at C4 is axial. Based on the ^{1}H- and ^{19}F-NMR spectra (fig. S12), the compound corresponds to the racemate in table S1 (protonated form highlighted in blue: H-F3 and H-F7; deprotonated form highlighted in green: F3 and F7).

Analgesia

We examined local in vivo analgesic effects at peripheral opioid receptors in more detail in the CFA model. When injected into inflamed paws, both fentanyl and NFEPP (0.5-2 μg i.pl.) produced dose-dependent PPT elevations in injected paws (fig. S7, A and B). At doses of 1.5–2 μg i.pl., fentanyl evoked significant PPT increases also in contralateral noninflamed paws (fig. S7C), whereas no such effects were observed with NFEPP (fig. S7D). The analgesic effects of fentanyl in injured paws were only partially reversed by i.pl. co-injected NLXM (fig. S7E), indicating both centrally and peripherally mediated analgesia. Conversely, the injury-restricted analgesic effect induced by i.pl. NFEPP was abolished completely by co-injection of NLXM (fig. S7F).

To identify the opioid receptor types mediating the observed analgesia, selective mu- (CTOP), delta- (ICI 174,864) and kappa- (norBNI) opioid receptor antagonists were co-injected with agonists into inflamed paws. The effects of i.pl. fentanyl and NFEPP (both at 2 μg) were reversed only by CTOP (8 μg i.pl.) (fig. S8, A and B), demonstrating selective MOR activation.

In the model of acute incisional pain, rats developed hyperalgesia, allodynia and heat sensitivity, manifested by reduced PPT (fig. S9, A and D), PWT (fig. S9, B and E) and PWL (fig. S9, C and F) in injured compared to contralateral paws. Both fentanyl and NFEPP (4–16 μg/kg i.v.) dose-dependently increased PPT, PWT and PWL in injured paws (fig. S9, A to F; fig. S10, A to C). In contralateral noninjured paws, fentanyl also produced analgesic effects (fig. S9, B and C; fig. S10, A to C), whereas NFEPP was completely ineffective (fig. S9, D to F; fig. S10, A to C). At 16 μg/kg i.v., fentanyl, but not NFEPP, caused overt respiratory depression. Analgesia mediated by systemic fentanyl (12 μg/kg i.v.) was partially reversed by NLXM (50 μg) injected i.pl. into injured paws, indicating the activation of both peripheral and central opioid receptors (fig. S10, D to F). In contrast, the effects of NFEPP (12 μg/kg i.v.) were virtually abolished by NLXM (fig. S10, D to F).

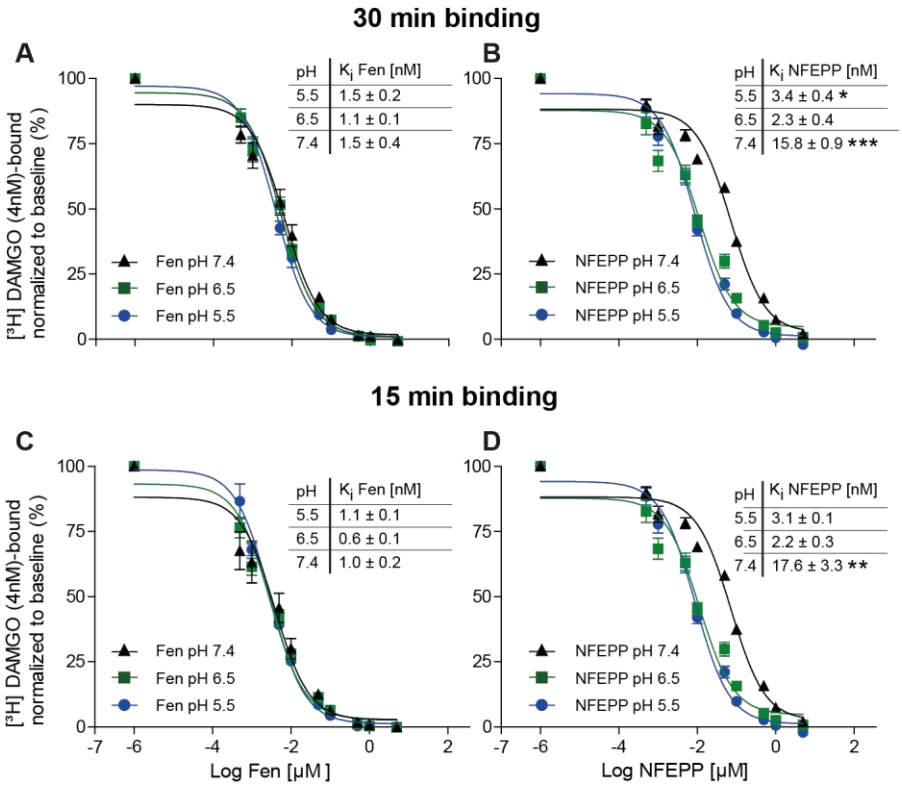

Fig. S1. Displacement of [³H]DAMGO binding by fentanyl and NFEPP at different incubation times.

(**A** and **B**) Fentanyl (Fen) and NFEPP incubation for 30 min or (**C** and **D**) 15 min displacing 4 nM [³H]DAMGO in membrane preparations from MOR-transfected HEK293 cells at pH 5.5, 6.5 and pH 7.4. **P* < 0.05, ***P* < 0.01, ****P* < 0.001 fentanyl vs NFEPP, two-way ANOVA and Bonferroni test (**A** and **B**), Kruskal-Wallis and Dunn's test (**C** and **D**) (means ± SEM).

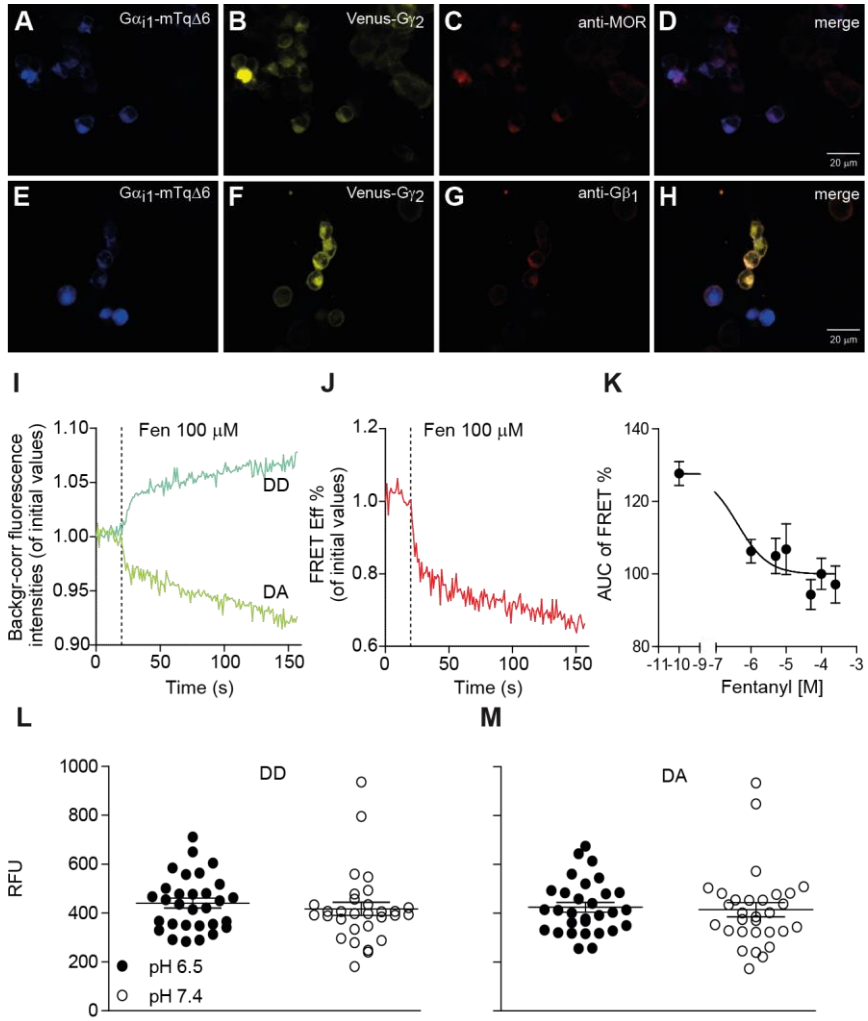

Fig. S2. Localization of MOR and G-protein subunits in HEK293 cells, and FRET assay.

(**A** to **H**) Co-localization (**D** and **H**) of Gαi1–mTqΔ6 (**A** and **E**) and Venus-Gγ2 (**B** and **F**) with MOR (**C**) or Gβ1 (**G**) shown by immunostaining of fixed cells transiently transfected with the respective proteins. (**I** and **J**) Stimulation of live MOR-transfected cells with fentanyl induced (**I**) fluorescence-based energy transfer from Venus-Gγ2 (green, donor excitation-acceptor emission: DA) to Gαi1-mTqΔ6 (cyan, donor excitation-donor emission: DD) resulting in a decrease of (**J**) FRET efficiency. Time of application (20 s) is indicated by dotted lines. Traces show a representative region of interest. (**K**) Dose-dependency of fentanyl effect as measured by AUC of FRET% (n = 4 to 14). (**L** and **M**) Prior to pH-dependent experiments, raw initial fluorescence intensities (relative fluorescence units, RFU) of Gαi1-mTqΔ6 and Venus-Gγ2 were compared at physiological (7.4) and low (6.5) extracellular pH in live cells. $P > 0.05$ pH 7.4 vs 6.5, Wilcoxon test. Data are raw intensities corrected for background. Lines and error bars represent means ± SEM (n = 30, averaging 366-409 cells).

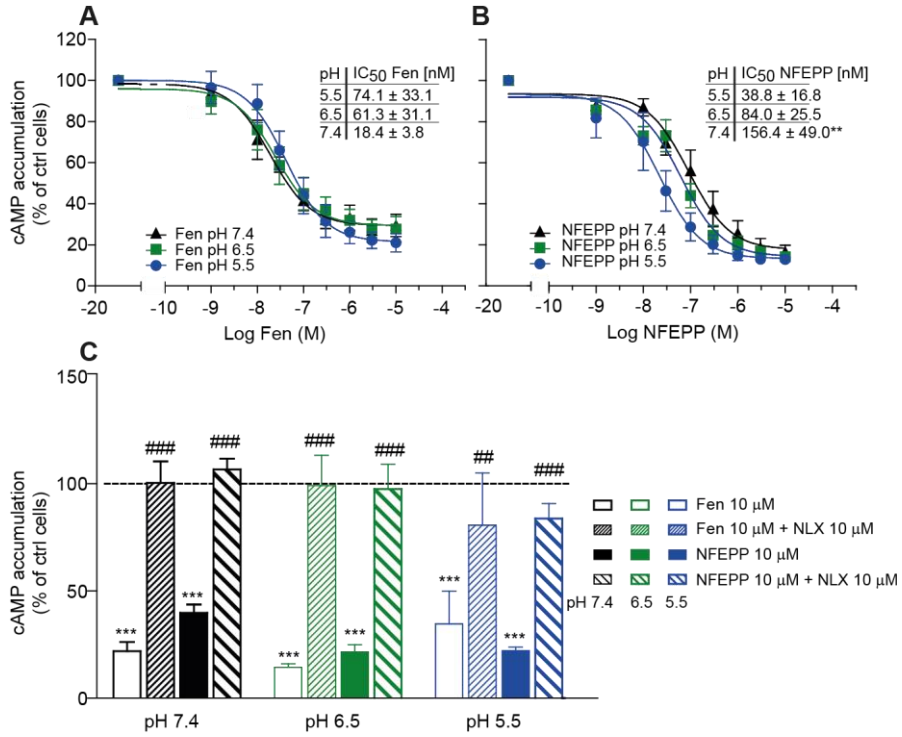

Fig. S3. NFEPP inhibits cAMP preferentially at low pH *via* MOR.

(A and B) Inhibition of FSK/IBMX-stimulated adenylyl cyclase by (A) fentanyl or (B) NFEPP incubated for 20 min at pH 5.5, 6.5 and 7.4. Inserts show IC50 (n = 6 to 8). (B) **P < 0.01 fentanyl vs NFEPP; two-way ANOVA and Bonferroni test. (C) Co-application of the highest doses of fentanyl or NFEPP with naloxone (NLX) at pH 5.5, 6.5 and 7.4 (n = 5 to 6). ***P < 0.001 fentanyl or NFEPP vs 100% (FSK/IBMX); ##P < 0.01, ###P <0.001 fentanyl or NFEPP vs fentanyl + NLX or NFEPP + NLX, respectively. Two-way ANOVA and Bonferroni test (means ± SEM).

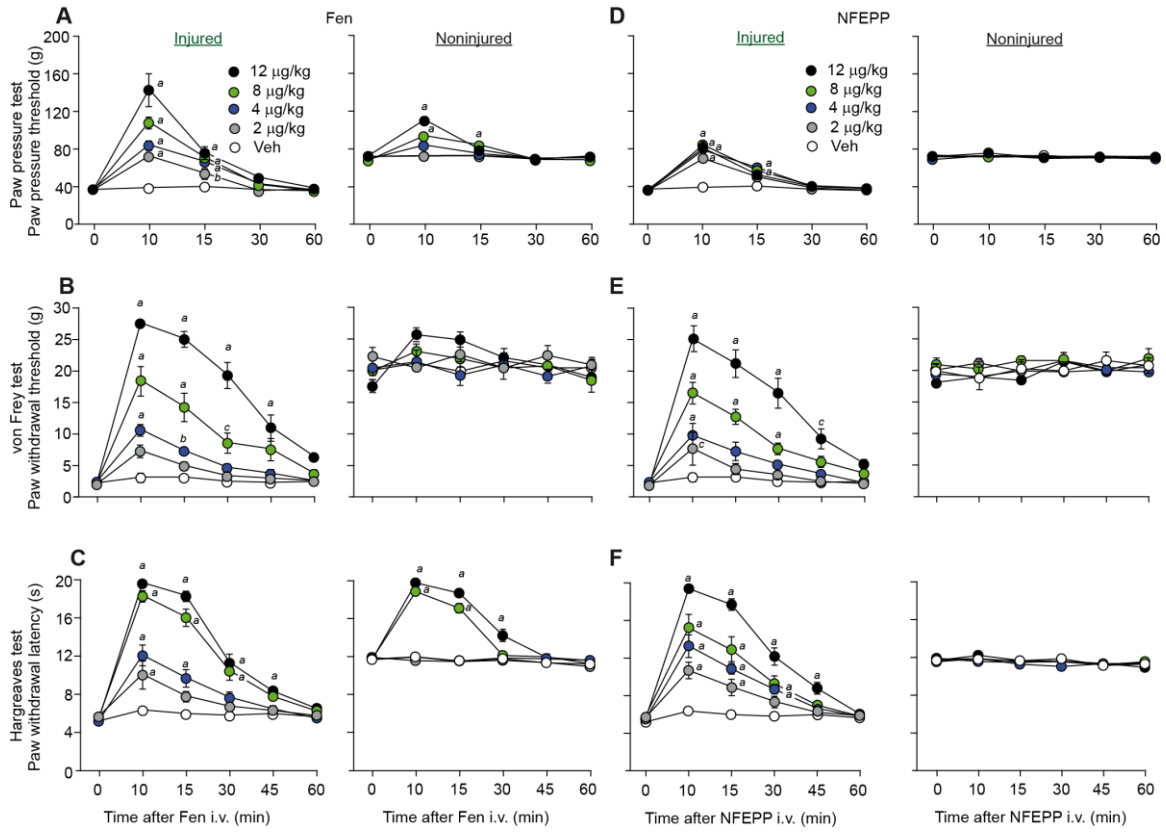

Fig. S4. Dose- and time-dependent analgesic effects produced by systemic fentanyl and NFEPP in the CFA model.

(**A** and **D**) Measurements of PPT, (**B** and **E**) PWT and (**C** and **F**) PWL in inflamed (left panels) and contralateral noninflamed paws (right panels) following i.v. injection of fentanyl (**A** to **C**) and NFEPP (**D** to **F**). c$P < 0.05$, b$P < 0.01$, a$P < 0.001$ vs vehicle (Veh), two-way RM ANOVA and Bonferroni test (means ± SEM; $n = 8$ to 9).

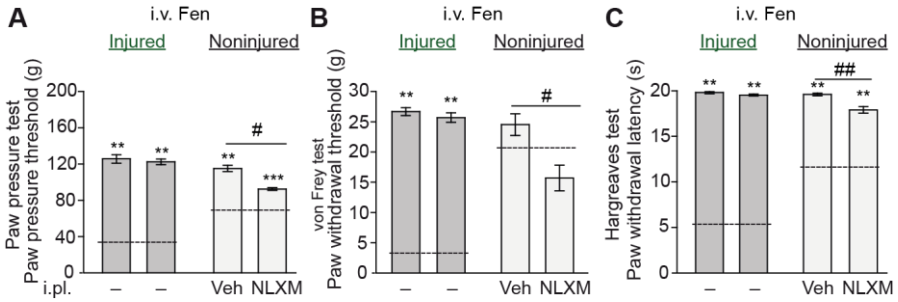

Fig. S5. Analgesic effects of systemic fentanyl in noninjured paws are partially mediated by peripheral opioid receptors in the CFA model.

Effect of NLXM (50 μg) injected i.pl. into noninjured paws after i.v. fentanyl (12 μg/kg) on (**A**) PPT, (**B**) PWT and (**C**) PWL in inflamed (injured) and noninjured paws compared to vehicle. ***P* < 0.01, ****P* < 0.001 vs baseline (dashed lines), Wilcoxon test; #*P* < 0.05, ##*P* < 0.01 NLXM vs vehicle, Mann-Whitney test (means ± SEM; *n* = 7 to 9).

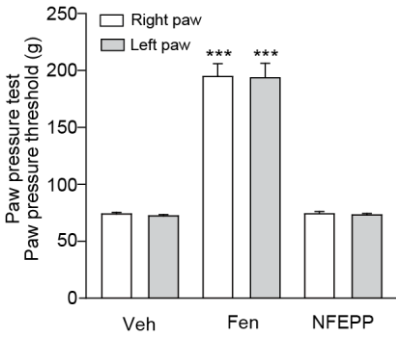

Fig. S6. Lack of analgesic effects of systemic NFEPP in naïve animals.

Effect of fentanyl, NFEPP (both at 12 μg/kg; i.v.) or vehicle on PPT values at 10 min after injection in naïve animals. ***$P < 0.001$ vs vehicle, Mann-Whitney test (means ± SEM; $n = 9$).

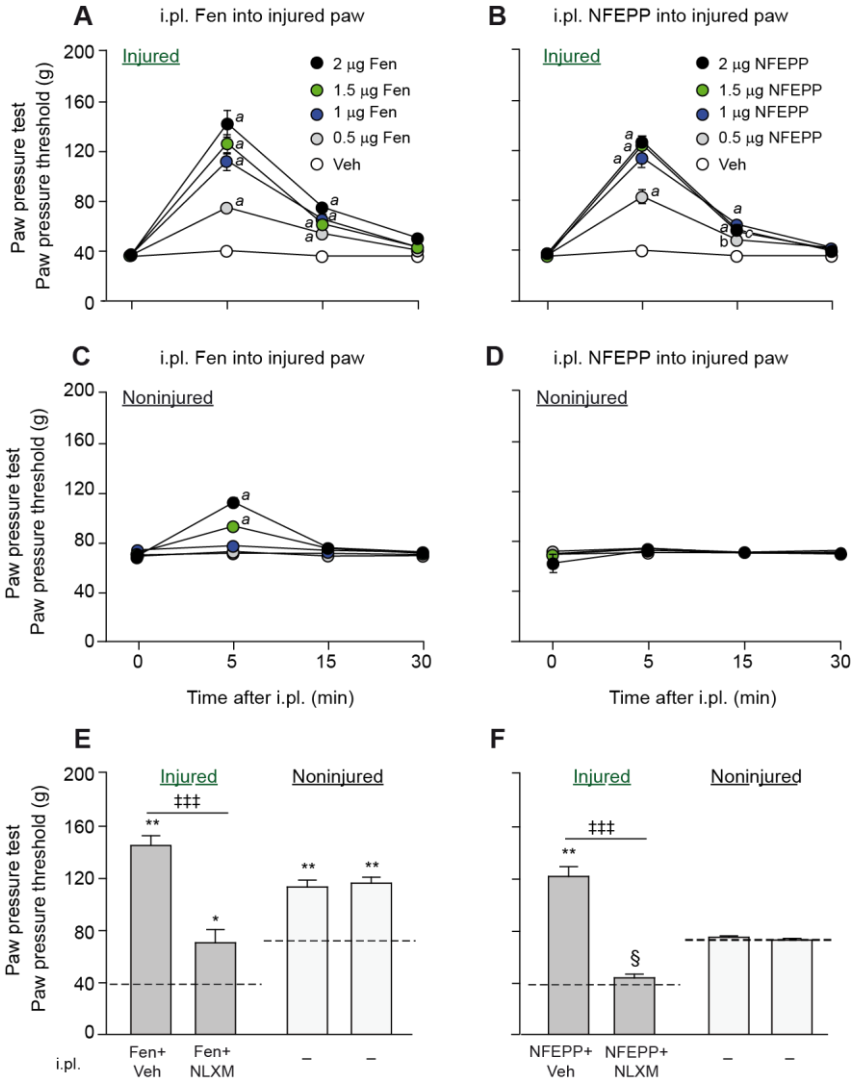

Fig. S7. Exclusive activation of peripheral opioid receptors by i.pl. NFEPP in the CFA model.

(**A** to **D**) Dose- and time-dependent PPT elevations in inflamed (injured) and noninjured paws after i.pl. injection of (**A** and **C**) fentanyl and (**B** and **D**) NFEPP into inflamed paws. c$P < 0.05$, b$P < 0.01$, a$P < 0.001$ vs vehicle, two-way RM ANOVA and Bonferroni test. (**E** to **F**) Effects at 5 min after i.pl. co-injection of (**E**) fentanyl (2 µg) or (**F**) NFEPP (2 µg) with NLXM (8 µg) into injured paws. *$P < 0.05$, #$P < 0.01$ vs baseline (dashed lines), Wilcoxon test; ‡‡‡$P < 0.001$ vs vehicle, Mann-Whitney test; §$P < 0.05$ vs fentanyl + NLXM injection into inflamed paws, Mann-Whitney test (means ± SEM; $n = 8$ to 9).

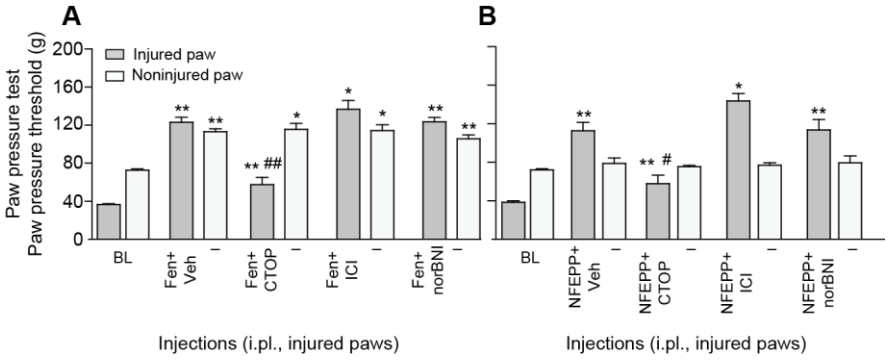

Fig. S8. Analgesic effects of fentanyl and NFEPP are selectively mediated by MOR.
(**A**) Effects on PPT at 5 min after co-injection of fentanyl and (**B**) NFEPP (both at 2 μg i.pl.) with vehicle or antagonists to mu- (CTOP; 8 μg i.pl.), but not to delta- (ICI; 5 μg i.pl.) or kappa- (norBNI; 50 μg i.pl.) opioid receptors into CFA-inflamed paws. **P* < 0.05, ***P* < 0.01 vs baseline (BL), Wilcoxon test; #*P* < 0.05, ##*P* < 0.01 vs vehicle, Kruskal-Wallis and Dunn's test (means ± SEM; *n* = 6 to 9).

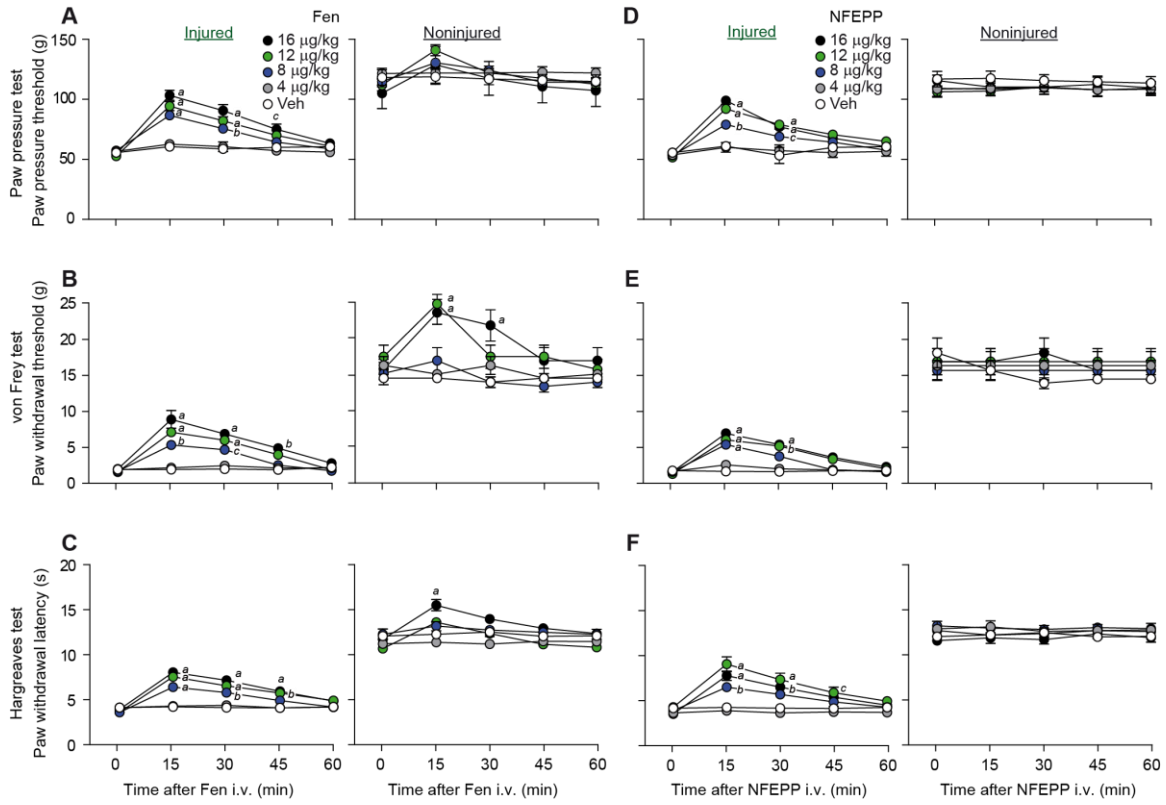

Fig. S9. Dose- and time-dependent analgesia induced by systemic fentanyl and NFEPP in post-incisional pain.

(**A** to **C**) Dose- and time-dependency of i.v. fentanyl and (**D** to **F**) NFEPP (both i.v.) effects on (A and D) mechanical hyperalgesia (PPT), (B and E) allodynia (PWT) and (C and F) thermal sensitivity (PWL) in injured (left panels) and noninjured (right panels) paws of rats with unilateral hindpaw incision. c$P < 0.05$, b$P < 0.01$, a$P < 0.001$ vs vehicle, two-way RM ANOVA and Bonferroni test (means ± SEM; n = 6-9).

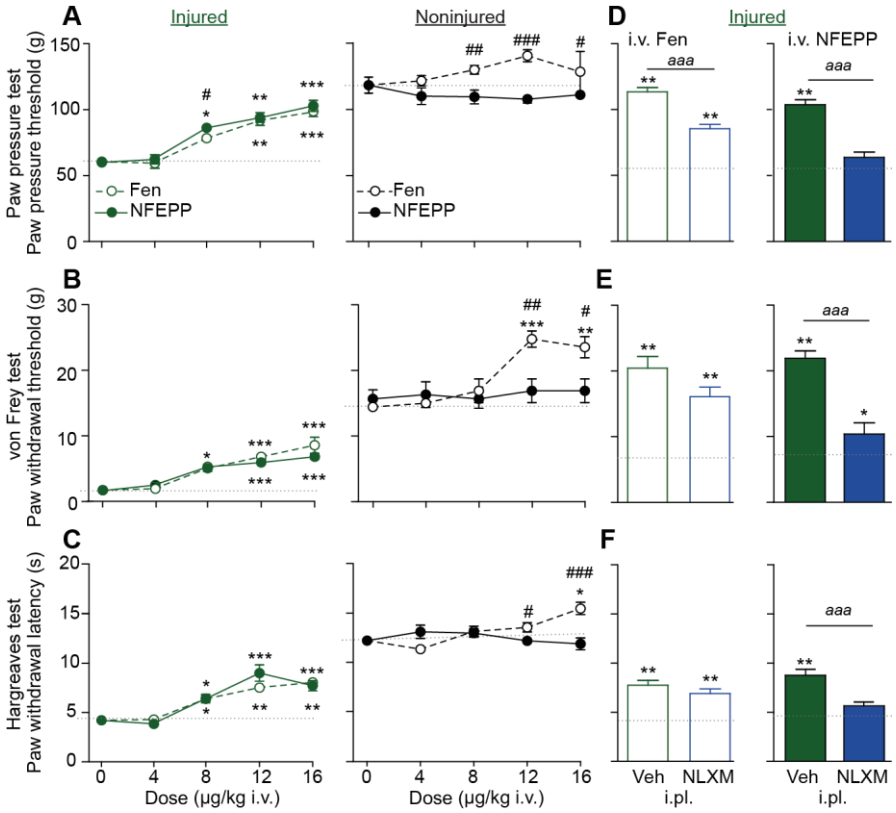

Fig. S10. Systemic NFEPP reduces pain selectively in incised paws *via* peripheral MOR.

(**A** to **F**) Effects at 15 min after i.v. fentanyl or NFEPP on (A) mechanical hyperalgesia, (B) allodynia and (C) heat sensitivity in incised (left panels) and nonincised paws (right panels). (D to F) Contribution of peripheral MOR to analgesia, assessed 15 min after i.v. injection of fentanyl (left panels) or NFEPP (right panels) (each at 12 µg/kg) with NLXM (50 µg) or vehicle injected i.pl. into injured paws. #P < 0.05, ##P < 0.01, ###P < 0.001 fentanyl vs NFEPP, aaaP < 0.001 vs NLXM, Mann-Whitney (A to C) or unpaired t-test (D to F; *P < 0.05, **P < 0.01, ***P < 0.001 vs dotted grey lines, representing "0 µg/kg" in A to C (Kruskal-Wallis and Dunn's test) or baseline in D to F (Wilcoxon test) (means ± SEM; *n* = 6 to 9).

Agilent LC/MS Data Browser Report

Target Mass	Formula	Found	%MSPurity	Peak#
355	N/A	**Yes**	0,0	14, 15, 19, 20, 21, 22

Peak#	Time	Area%			Target Mass	Peak Purity			Area	Amount	Start Time
		DAD1 254	MSD1 TIC+	MSD2 TIC-		DAD1 254	MSD1 TIC+	MSD2 TIC-			
1	0,12	4,06				N/A			0,98E1		0,09
2	0,36		0,09				N/A		0,91E5		0,30
3	0,56			1,51				N/A	0,62E4		0,51
4	0,64		0,11				N/A		1,06E5		0,56
5	0,84			5,31				N/A	2,17E4		0,76
6	1,11		0,13	2,54			N/A	N/A	1,04E4		1,03
7	1,21		0,30				N/A		2,98E5		1,08
8	1,39		0,40				N/A		0,4E6		1,32
9	1,69			2,58				N/A	1,06E4		1,63
10	1,82		0,17	2,33			N/A	N/A	0,95E4		1,76
11	1,95		0,06				N/A		0,62E5		1,88
12	2,02		0,07				N/A		0,7E5		1,98
13	2,30			5,62				N/A	2,3E4		2,26
14	2,65	78,71	7,52	6,76	**355**	N/A	N/A	N/A	1,89E2		2,59
15	2,87		50,77	1,55	**(355)**		N/A	N/A	0,64E4		2,81
16	3,66			1,56				N/A	0,64E4		3,57
17	3,88			0,88				N/A	0,36E4		3,79
18	4,06			18,03				N/A	0,74E5		3,99
19	4,31		6,35	40,35	**355**		N/A	N/A	1,65E5		4,25
20	4,46		4,02		(355)		N/A		0,4E7		4,38
21	4,60		1,80		(355)		N/A		1,8E6		4,56
22	4,77		3,46		(355)		N/A		0,35E7		4,65
23	4,87		2,27				N/A		2,28E6		4,82
24	5,02		2,51				N/A		2,51E6		4,94
25	5,12		2,08				N/A		2,08E6		5,07
26	5,22		1,87				N/A		1,87E6		5,17
27	5,40		4,41	2,20			N/A	N/A	0,9E4		5,32
28	5,59		11,59	8,78			N/A	N/A	0,36E5		5,47
29	5,80	17,23				N/A			0,41E2		5,51

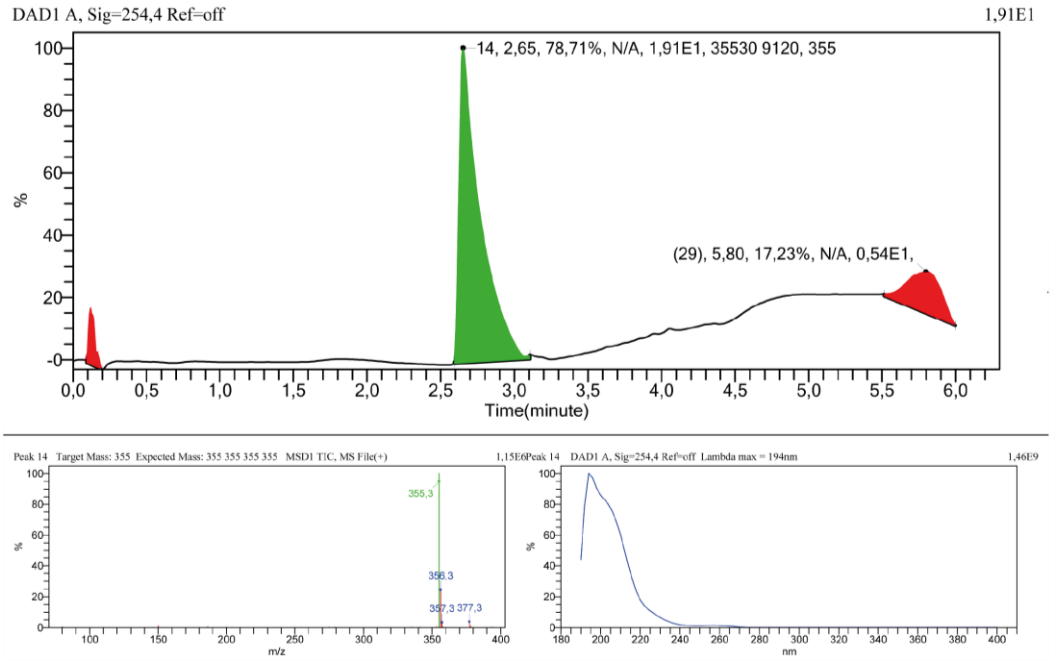

Fig. S11. HPLC/MS for mass characterization of NFEPP.

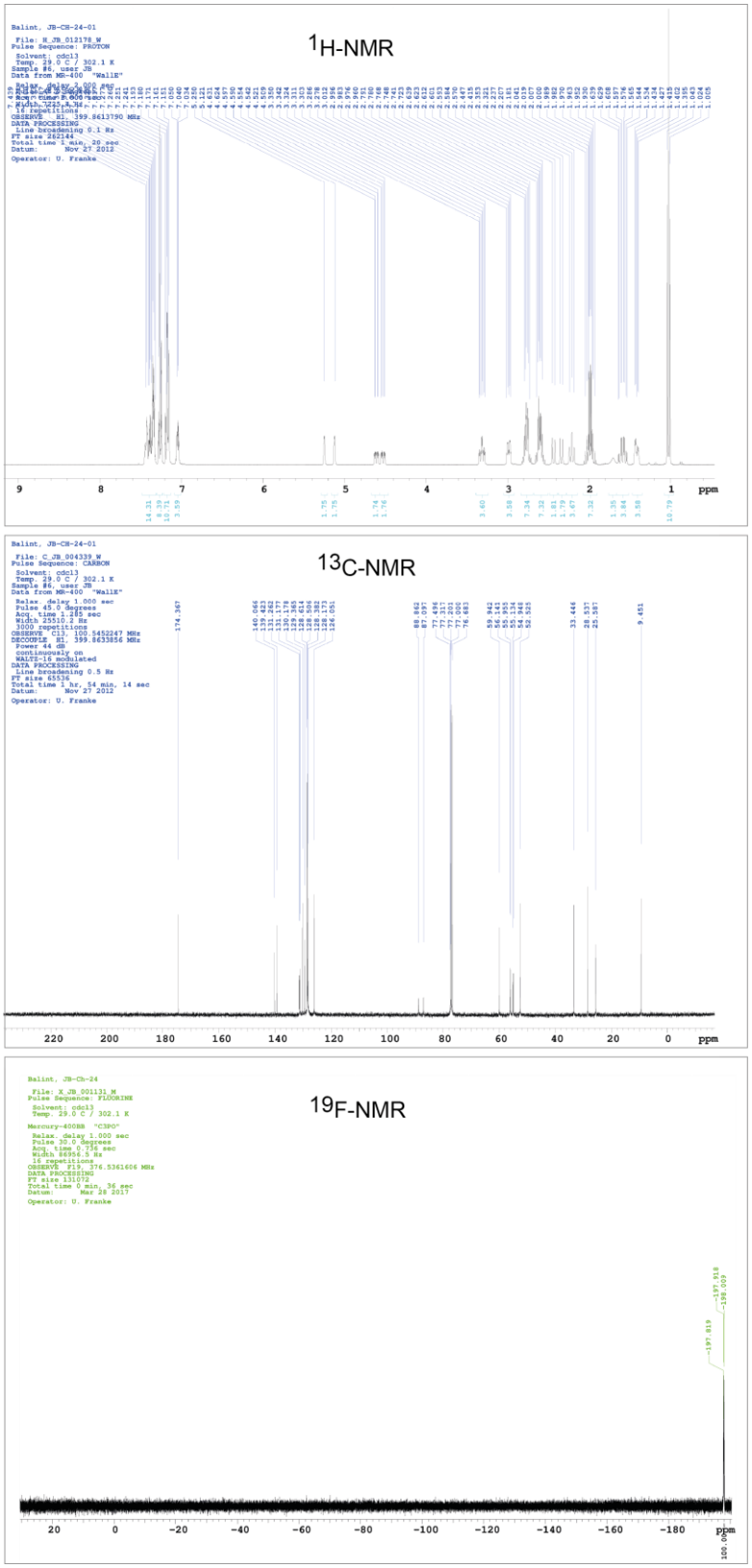

Fig. S12. ^{1}H-NMR, ^{13}C-NMR, ^{19}F-NMR spectra of NFEPP.

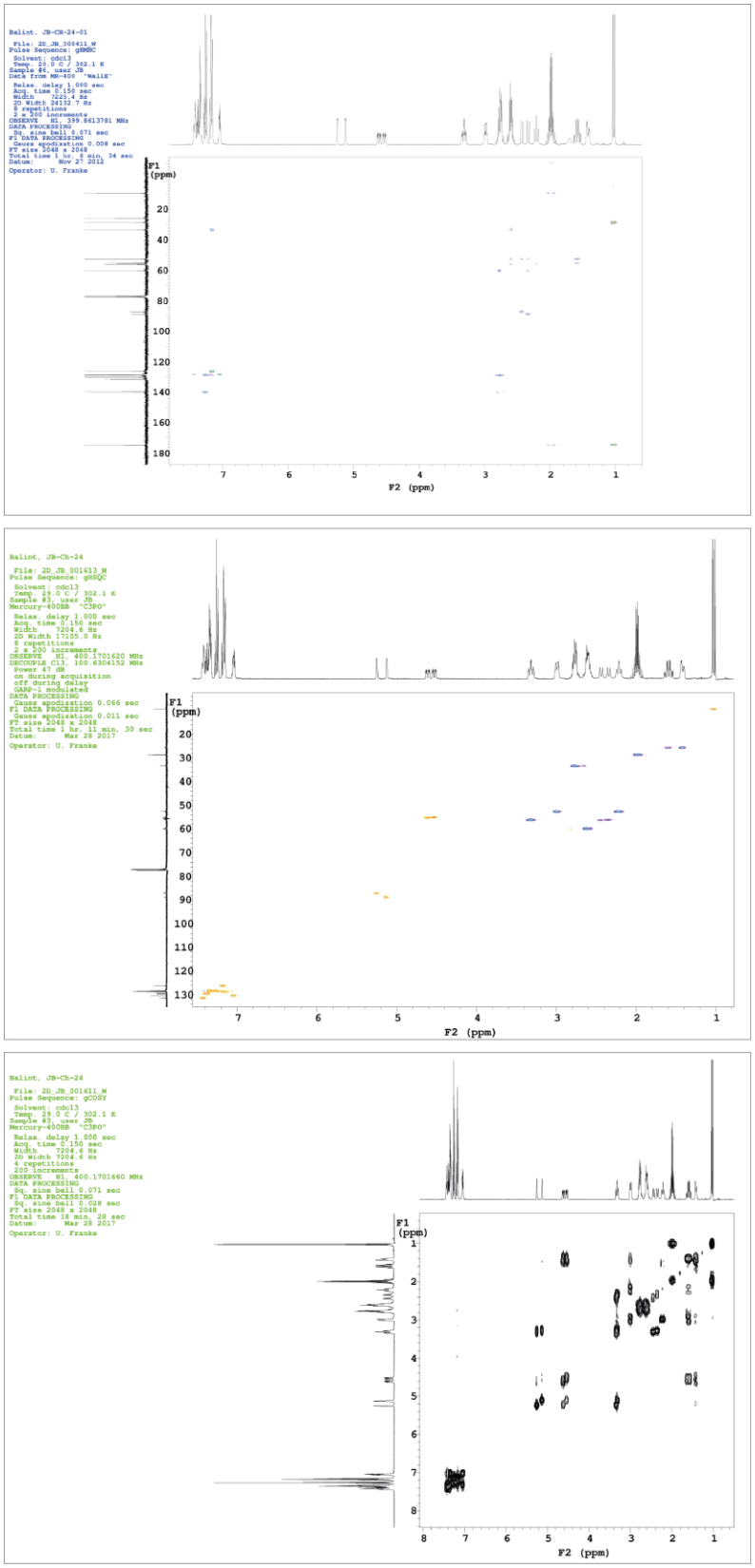

Fig. S13. HMBC, HSQC and COSY spectra of NFEPP.

Table S1. Estimated pKa and Gibbs free energy values of fluorinated fentanyl derivatives.

Estimated pK_a and Gibbs free energy values of fluorinated fentanyl derivatives in protonated (H-F1 to H-F13) and deprotonated forms (F3, F4, F6, F7) under injured (acidic) and noninjured (neutral) conditions. Highlighted are ΔG values of NFEPP under injured (blue) and noninjured (green) conditions. ΔG values of protonated NFEPP under noninjured conditions are shown in italics.

Molecule	Replaced Hydrogen (Index)	Estimated pKa	Stereo-isomers	$\Delta G_{injured}$ (kJ/mol)	$\Delta G_{noninjured}$ (kJ/mol)
H-Fen	-	9.82		-10,7	-14,7
H-F1	1	3.56	F1*	-11,9	-21,9
H-F2	2	2.61	F1*	-15,8	-15,9
H-F3	3	6.73	F3*	-20,1	*-17,9*
H-F4	4	7.85	F3*	-16,8	*-12,0*
H-F5	5	7.77		-19,2	-13,4
H-F6	6	7.66	F3*	-16,3	*-11,1*
H-F7	7	6.93	F3*	-19,5	*-9,8*
H-F8	8	3.63	F1*	-14,2	-9,2
H-F9	9	3.48	F1*	-24,4	-7,3
H-F10	10	2.06	F2*	-21,9	-20,2
H-F11	11	3.38	F2*	-16,4	-30,8
H-F12	12	7.77		-17,3	-9,6
H-F13	13	2.65		-9,6	-8,9
Fen				9,5	2,4
F3				-18,0	-14,9
F4				-0,6	5,9
F6				-1,2	11,8
F7				-10,9	2,1

References and Notes

1. V. J. Dzau, P. A. Pizzo, Relieving pain in America: Insights from an Institute of Medicine committee. *JAMA* **312**, 1507–1508 (2014). doi:10.1001/jama.2014.12986 Medline

2. N. Bhala, J. Emberson, A. Merhi, S. Abramson, N. Arber, J. A. Baron, C. Bombardier, C. Cannon, M. E. Farkouh, G. A. FitzGerald, P. Goss, H. Halls, E. Hawk, C. Hawkey, C. Hennekens, M. Hochberg, L. E. Holland, P. M. Kearney, L. Laine, A. Lanas, P. Lance, A. Laupacis, J. Oates, C. Patrono, T. J. Schnitzer, S. Solomon, P. Tugwell, K. Wilson, J. Wittes, C. Baigent; Coxib and traditional NSAID Trialists' (CNT) Collaboration, Vascular and upper gastrointestinal effects of non-steroidal anti-inflammatory drugs: Meta-analyses of individual participant data from randomised trials. *Lancet* **382**, 769–779 (2013). doi:10.1016/S0140-6736(13)60900-9 Medline

3. R. M. Califf, J. Woodcock, S. Ostroff, A proactive response to prescription opioid abuse. *N. Engl. J. Med.* **374**, 1480–1485 (2016). doi:10.1056/NEJMsr1601307 Medline

4. I. D. Pogozheva, M. J. Przydzial, H. I. Mosberg, Homology modeling of opioid receptor-ligand complexes using experimental constraints. *AAPS J.* **7**, E434–E448 (2005). doi:10.1208/aapsj070243 Medline

5. L. Dosen-Micovic, M. Ivanovic, V. Micovic, Steric interactions and the activity of fentanyl analogs at the μ-opioid receptor. *Bioorg. Med. Chem.* **14**, 2887–2895 (2006). doi:10.1016/j.bmc.2005.12.010 Medline

6. N. Richards, S. B. McMahon, Targeting novel peripheral mediators for the treatment of chronic pain. *Br. J. Anaesth.* **111**, 46–51 (2013). doi:10.1093/bja/aet216 Medline

7. R. Baron, G. Hans, A. H. Dickenson, Peripheral input and its importance for central sensitization. *Ann. Neurol.* **74**, 630–636 (2013). doi:10.1002/ana.24017 Medline

8. J. Sawynok, J. Liu, Contributions of peripheral, spinal, and supraspinal actions to analgesia. *Eur. J. Pharmacol.* **734**, 114–121 (2014). doi:10.1016/j.ejphar.2014.04.006 Medline

9. I. Tabas, C. K. Glass, Anti-inflammatory therapy in chronic disease: Challenges and opportunities. *Science* **339**, 166–172 (2013). doi:10.1126/science.1230720 Medline

10. P. Holzer, Acid-sensitive ion channels and receptors. *Handb. Exp. Pharmacol.* **194**, 283–332 (2009). doi:10.1007/978-3-540-79090-7_9 Medline

11. C. Stein, Opioid receptors. *Annu. Rev. Med.* **67**, 433–451 (2016). doi:10.1146/annurev-med-062613-093100 Medline

12. C. Jagla, P. Martus, C. Stein, Peripheral opioid receptor blockade increases postoperative morphine demands—a randomized, double-blind, placebo-controlled trial. *Pain* **155**, 2056–2062 (2014). doi:10.1016/j.pain.2014.07.011 Medline

13. C. Gaveriaux-Ruff, C. Nozaki, X. Nadal, X. C. Hever, R. Weibel, A. Matifas, D. Reiss, D. Filliol, M. A. Nassar, J. N. Wood, R. Maldonado, B. L. Kieffer, Genetic ablation of delta opioid receptors in nociceptive sensory neurons increases chronic pain and abolishes opioid analgesia. *Pain* **152**, 1238–1248 (2011). doi:10.1016/j.pain.2010.12.031 Medline

14. R. Weibel, D. Reiss, L. Karchewski, O. Gardon, A. Matifas, D. Filliol, J. A. J. Becker, J. N. Wood, B. L. Kieffer, C. Gaveriaux-Ruff, Mu opioid receptors on primary afferent nav1.8 neurons contribute to opiate-induced analgesia: Insight from conditional knockout mice. *PLOS ONE* **8**, e74706 (2013). doi:10.1371/journal.pone.0074706 Medline

15. S. R. Childers, Opiate-inhibited adenylate cyclase in rat brain membranes depleted of G_s-stimulated adenylate cyclase. *J. Neurochem.* **50**, 543–553 (1988). doi:10.1111/j.1471-4159.1988.tb02945.x Medline

16. M. G. Ludwig, M. Vanek, D. Guerini, J. A. Gasser, C. E. Jones, U. Junker, H. Hofstetter, R. M. Wolf, K. Seuwen, Proton-sensing G-protein-coupled receptors. *Nature* **425**, 93–98 (2003). doi:10.1038/nature01905 Medline

17. X. Deupi, B. K. Kobilka, Energy landscapes as a tool to integrate GPCR structure, dynamics, and function. *Physiology (Bethesda)* **25**, 293–303 (2010). doi:10.1152/physiol.00002.2010 Medline

18. K. P. Hofmann, P. Scheerer, P. W. Hildebrand, H.-W. Choe, J. H. Park, M. Heck, O. P. Ernst, A G protein-coupled receptor at work: The rhodopsin model. *Trends Biochem. Sci.* **34**, 540–552 (2009). doi:10.1016/j.tibs.2009.07.005 Medline

19. L. Ye, N. Van Eps, M. Zimmer, O. P. Ernst, R. S. Prosser, Activation of the A2A adenosine G-protein-coupled receptor by conformational selection. *Nature* **533**, 265–268 (2016). doi:10.1038/nature17668 Medline

20. J. G. Li, C. Chen, J. Yin, K. Rice, Y. Zhang, D. Matecka, J. K. de Riel, R. L. DesJarlais, L.-Y. Liu-Chen, ASP147 in the third transmembrane helix of the rat μ opioid receptor forms ion-pairing with morphine and naltrexone. *Life Sci.* **65**, 175–185 (1999). doi:10.1016/S0024-3205(99)00234-9 Medline

21. W. Huang, A. Manglik, A. J. Venkatakrishnan, T. Laeremans, E. N. Feinberg, A. L. Sanborn, H. E. Kato, K. E. Livingston, T. S. Thorsen, R. C. Kling, S. Granier, P. Gmeiner, S. M. Husbands, J. R. Traynor, W. I. Weis, J. Steyaert, R. O. Dror, B. K. Kobilka, Structural insights into μ-opioid receptor activation. *Nature* **524**, 315–321 (2015). doi:10.1038/nature14886 Medline

22. R. Sounier, C. Mas, J. Steyaert, T. Laeremans, A. Manglik, W. Huang, B. K. Kobilka, H. Déméné, S. Granier, Propagation of conformational changes during μ-opioid receptor activation. *Nature* **524**, 375–378 (2015). doi:10.1038/nature14680 Medline

23. A. Manglik, A. C. Kruse, T. S. Kobilka, F. S. Thian, J. M. Mathiesen, R. K. Sunahara, L. Pardo, W. I. Weis, B. K. Kobilka, S. Granier, Crystal structure of the μ-opioid receptor bound to a morphinan antagonist. *Nature* **485**, 321–326 (2012). doi:10.1038/nature10954 Medline

24. M. A. Schumacher, A. I. Basbaum, W. L. Way, in *Basic and Clinical Pharmacology*, B. G. Katzung, S. B. Masters, A. J. Trevor, Eds. (McGraw-Hill Medical, New York, 2009), pp. 531–552.

25. M. Filizola, H. O. Villar, G. H. Loew, Differentiation of delta, mu, and kappa opioid receptor agonists based on pharmacophore development and computed physicochemical properties. *J. Comput. Aided Mol. Des.* **15**, 297–307 (2001). doi:10.1023/A:1011187320095 Medline

26. J. R. Deschamps, J. L. Flippen-Anderson, C. George, X-ray studies on ligands. *Biopolymers* **66**, 287–293 (2002). doi:10.1002/bip.10308 Medline

27. R. L. Thurlkill, D. A. Cross, J. M. Scholtz, C. N. Pace, pK_a of fentanyl varies with temperature: Implications for acid-base management during extremes of body temperature. *J. Cardiothorac. Vasc. Anesth.* **19**, 759–762 (2005). doi:10.1053/j.jvca.2004.11.039 Medline

28. S. D. Roy, G. L. Flynn, Solubility behavior of narcotic analgesics in aqueous media: Solubilities and dissociation constants of morphine, fentanyl, and sufentanil. *Pharm. Res.* **6**, 147–151 (1989). doi:10.1023/A:1015932610010 Medline

29. D. R. Brown, L. I. Goldberg, The use of quaternary narcotic antagonists in opiate research. *Neuropharmacology* **24**, 181–191 (1985). doi:10.1016/0028-3908(85)90072-3 Medline

30. S. Karimi, M. Karami, H. Zardooz, S. H. Salimi, H. Sahraei, Biphasic effects of naloxone in the rats receiving morphine overdose a place preference study. *Iran. J. Pharm. Res.* **10**, 605–610 (2011). Medline

31. C. Canestrelli, N. Marie, F. Noble, Rewarding or aversive effects of buprenorphine/naloxone combination (Suboxone) depend on conditioning trial duration. *Int. J. Neuropsychopharmacol.* **17**, 1367–1373 (2014). doi:10.1017/S146114571400025X Medline

32. E. R. Viscusi, L. Webster, M. Kuss, S. Daniels, J. A. Bolognese, S. Zuckerman, D. G. Soergel, R. A. Subach, E. Cook, F. Skobieranda, A randomized, phase 2 study investigating TRV130, a biased ligand of the μ-opioid receptor, for the intravenous treatment of acute pain. *Pain* **157**, 264–272 (2016). doi:10.1097/j.pain.0000000000000363 Medline

33. H. Lu, X. Chen, C. G. Zhan, First-principles calculation of pK_a for cocaine, nicotine, neurotransmitters, and anilines in aqueous solution. *J. Phys. Chem. B* **111**, 10599–10605 (2007). doi:10.1021/jp072917r Medline

34. M. J. Frisch, G. W. Trucks, H. B. Schlegel, G. E. Scuseria, M.A. Robb, J. R. Cheeseman, G. Scalmani, V. Barone, B. Mennucci, G. A. Petersson, H. Nakatsuji, M. Caricato, X. Li, H. P. Hratchian, A. F. Izmaylov, J. Bloino, G. Zheng, J. L. Sonnenberg, M. Hada, M. Ehara, K. Toyota, R. Fukuda, J. Hasegawa, M. Ishida, T. Nakajima, Y. Honda, O. Kitao, H. Nakai, T. Vreven, J. A. Montgomery, Jr., J. E. Peralta, F. Ogliaro, M. Bearpark, J. J. Heyd, E. Brothers, K. N. Kudin, V. N. Staroverov, R. Kobayashi, J. Normand, K. Raghavachari, A. Rendell, J. C. Burant, S. S. Iyengar, J. Tomasi, M. Cossi, N. Rega, J. M. Millam, M. Klene, J. E. Knox, J. B. Cross, V. Bakken, C. Adamo, J. Jaramillo, R. Gomperts, R. E.

Stratmann, O. Yazyev, A. J. Austin, R. Cammi, C. Pomelli, J. W. Ochterski, R. L. Martin, K. Morokuma, V. G. Zakrzewski, G. A. Voth, P. Salvador, J. J. Dannenberg, S. Dapprich, A. D. Daniels, Ö. Farkas, J. B. Foresman, J. V. Ortiz, J. Cioslowski, D. J. Fox, Gaussian 09, Revision A.1 (Gaussian, Inc., Wallingford, CT, 2009).

35. J. Wang, R. M. Wolf, J. W. Caldwell, P. A. Kollman, D. A. Case, Development and testing of a general amber force field. *J. Comput. Chem.* **25**, 1157–1174 (2004). doi:10.1002/jcc.20035 Medline

36. J. Wang, W. Wang, P. A. Kollman, D. A. Case, Automatic atom type and bond type perception in molecular mechanical calculations. *J. Mol. Graph. Model.* **25**, 247–260 (2006). doi:10.1016/j.jmgm.2005.12.005 Medline

37. A. Jakalian, B. L. Bush, D. B. Jack, C. I. Bayly, Fast, efficient generation of high-quality atomic charges. AM1-BCC model: I. Method. *J. Comput. Chem.* **21**, 132–146 (2000). doi:10.1002/(SICI)1096-987X(20000130)21:2<132:AID-JCC5>3.0.CO;2-P

38. A. Jakalian, D. B. Jack, C. I. Bayly, Fast, efficient generation of high-quality atomic charges. AM1-BCC model: II. Parameterization and validation. *J. Comput. Chem.* **23**, 1623–1641 (2002). doi:10.1002/jcc.10128 Medline

39. N. Guex, M. C. Peitsch, SWISS-MODEL and the Swiss-PdbViewer: An environment for comparative protein modeling. *Electrophoresis* **18**, 2714–2723 (1997). doi:10.1002/elps.1150181505 Medline

40. K. Lindorff-Larsen, S. Piana, K. Palmo, P. Maragakis, J. L. Klepeis, R. O. Dror, D. E. Shaw, Improved side-chain torsion potentials for the Amber ff99SB protein force field. *Proteins* **78**, 1950–1958 (2010). Medline

41. V. Durmaz, S. Schmidt, P. Sabri, C. Piechotta, M. Weber, Hands-off linear interaction energy approach to binding mode and affinity estimation of estrogens. *J. Chem. Inf. Model.* **53**, 2681–2688 (2013). doi:10.1021/ci400392p Medline

42. H. W. Horn, W. C. Swope, J. W. Pitera, J. D. Madura, T. J. Dick, G. L. Hura, T. Head-Gordon, Development of an improved four-site water model for biomolecular simulations: TIP4P-Ew. *J. Chem. Phys.* **120**, 9665–9678 (2004). doi:10.1063/1.1683075 Medline

43. B. Hess, C. Kutzner, D. van der Spoel, E. Lindahl, GROMACS 4: Algorithms for Highly Efficient, Load-Balanced, and Scalable Molecular Simulation. *J. Chem. Theory Comput.* **4**, 435–447 (2008). doi:10.1021/ct700301q Medline

44. G. Bussi, D. Donadio, M. Parrinello, Canonical sampling through velocity rescaling. *J. Chem. Phys.* **126**, 014101 (2007). doi:10.1063/1.2408420 Medline

45. M. Parrinello, A. Rahman, Polymorphic transitions in single crystals: A new molecular dynamics method. *J. Appl. Phys.* **52**, 7182–7190 (1981). doi:10.1063/1.328693

46. B. Hess, H. Bekker, H. J. C. Berendsen, J. G. E. M. Fraaije, LINCS: A linear constraint solver for molecular simulations. *J. Comput. Chem.* **18**, 1463–1472

(1997). doi:10.1002/(SICI)1096-987X(199709)18:12<1463:AID-JCC4>3.0.CO;2-H

47. U. Essmann, L. Perera, M. L. Berkowitz, T. Darden, H. Lee, L. G. Pedersen, A smooth particle mesh Ewald method. *J. Chem. Phys.* **103**, 8577–8593 (1995). doi:10.1063/1.470117

48. J. Aqvist, C. Medina, J. E. Samuelsson, A new method for predicting binding affinity in computer-aided drug design. *Protein Eng.* **7**, 385–391 (1994). doi:10.1093/protein/7.3.385 Medline

49. V. Spahn, C. Stein, C. Zöllner, Modulation of transient receptor vanilloid 1 activity by transient receptor potential ankyrin 1. *Mol. Pharmacol.* **85**, 335–344 (2014). doi:10.1124/mol.113.088997 Medline

50. M. Busch-Dienstfertig, C. A. Roth, C. Stein, Functional characteristics of the naked mole rat μ-opioid receptor. *PLOS ONE* **8**, e79121 (2013). doi:10.1371/journal.pone.0079121 Medline

51. V. Spahn, O. Fischer, J. Endres-Becker, M. Schäfer, C. Stein, C. Zöllner, Opioid withdrawal increases transient receptor potential vanilloid 1 activity in a protein kinase A-dependent manner. *Pain* **154**, 598–608 (2013). doi:10.1016/j.pain.2012.12.026 Medline

52. M. M. Bradford, A rapid and sensitive method for the quantitation of microgram quantities of protein utilizing the principle of protein-dye binding. *Anal. Biochem.* **72**, 248–254 (1976). doi:10.1016/0003-2697(76)90527-3 Medline

53. S. K. Gibson, A. G. Gilman, Gialpha and Gbeta subunits both define selectivity of G protein activation by alpha2-adrenergic receptors. *Proc. Natl. Acad. Sci. U.S.A.* **103**, 212–217 (2006). doi:10.1073/pnas.0509763102 Medline

54. S. Berlin, V. A. Tsemakhovich, R. Castel, T. Ivanina, C. W. Dessauer, T. Keren-Raifman, N. Dascal, Two distinct aspects of coupling between Gα(i) protein and G protein-activated K+ channel (GIRK) revealed by fluorescently labeled Gα(i3) protein subunits. *J. Biol. Chem.* **286**, 33223–33235 (2011). doi:10.1074/jbc.M111.271056 Medline

55. N. Audet, C. Galés, E. Archer-Lahlou, M. Vallières, P. W. Schiller, M. Bouvier, G. Pineyro, Bioluminescence resonance energy transfer assays reveal ligand-specific conformational changes within preformed signaling complexes containing delta-opioid receptors and heterotrimeric G proteins. *J. Biol. Chem.* **283**, 15078–15088 (2008). doi:10.1074/jbc.M707941200 Medline

56. C. Galés, J. J. J. Van Durm, S. Schaak, S. Pontier, Y. Percherancier, M. Audet, H. Paris, M. Bouvier, Probing the activation-promoted structural rearrangements in preassembled receptor-G protein complexes. *Nat. Struct. Mol. Biol.* **13**, 778–786 (2006). doi:10.1038/nsmb1134 Medline

57. P. Hein, F. Rochais, C. Hoffmann, S. Dorsch, V. O. Nikolaev, S. Engelhardt, C. H. Berlot, M. J. Lohse, M. Bünemann, Gs activation is time-limiting in initiating receptor-mediated signaling. *J. Biol. Chem.* **281**, 33345–33351 (2006). doi:10.1074/jbc.M606713200 Medline

58. M. J. Adjobo-Hermans, J. Goedhart, L. van Weeren, S. Nijmeijer, E. M. M. Manders, S. Offermanns, T. W. J. Gadella Jr., Real-time visualization of heterotrimeric G protein Gq activation in living cells. *BMC Biol.* **9**, 32 (2011). doi:10.1186/1741-7007-9-32 Medline

59. G. W. Gordon, G. Berry, X. H. Liang, B. Levine, B. Herman, Quantitative fluorescence resonance energy transfer measurements using fluorescence microscopy. *Biophys. J.* **74**, 2702–2713 (1998). doi:10.1016/S0006-3495(98)77976-7 Medline

60. Y. J. Shyu, C. D. Suarez, C. D. Hu, Visualization of ternary complexes in living cells by using a BiFC-based FRET assay. *Nat. Protoc.* **3**, 1693–1702 (2008). doi:10.1038/nprot.2008.157 Medline

61. M. Xia, V. Guo, R. Huang, S. A. Shahane, C. P. Austin, M. Nirenberg, S. K. Sharma, Inhibition of morphine-induced cAMP overshoot: A cell-based assay model in a high-throughput format. *Cell. Mol. Neurobiol.* **31**, 901–907 (2011). doi:10.1007/s10571-011-9689-y Medline

62. C. Stein, M. J. Millan, A. Herz, Unilateral inflammation of the hindpaw in rats as a model of prolonged noxious stimulation: Alterations in behavior and nociceptive thresholds. *Pharmacol. Biochem. Behav.* **31**, 445–451 (1988). doi:10.1016/0091-3057(88)90372-3 Medline

63. T. J. Brennan, E. P. Vandermeulen, G. F. Gebhart, Characterization of a rat model of incisional pain. *Pain* **64**, 493–501 (1996). doi:10.1016/0304-3959(95)01441-1 Medline

64. D. Nockemann, M. Rouault, D. Labuz, P. Hublitz, K. McKnelly, F. C. Reis, C. Stein, P. A. Heppenstall, The K($^{+}$) channel GIRK2 is both necessary and sufficient for peripheral opioid-mediated analgesia. *EMBO Mol. Med.* **5**, 1263–1277 (2013). doi:10.1002/emmm.201201980 Medline

65. K. Hargreaves, R. Dubner, F. Brown, C. Flores, J. Joris, A new and sensitive method for measuring thermal nociception in cutaneous hyperalgesia. *Pain* **32**, 77–88 (1988). doi:10.1016/0304-3959(88)90026-7 Medline

66. M. Moaddab, A. Haghparast, M. Hassanpour-Ezatti, Effects of reversible inactivation of the ventral tegmental area on the acquisition and expression of morphine-induced conditioned place preference in the rat. *Behav. Brain Res.* **198**, 466–471 (2009). doi:10.1016/j.bbr.2008.11.030 Medline

67. N. Roohi, A. Sarihi, S. Shahidi, M. Zarei, A. Haghparast, Microinjection of the mGluR5 antagonist MTEP into the nucleus accumbens attenuates the acquisition but not expression of morphine-induced conditioned place preference in rats. *Pharmacol. Biochem. Behav.* **126**, 109–115 (2014). doi:10.1016/j.pbb.2014.09.020 Medline